

## Border collision bifurcations at the change of state-space dimension

Sukanya Parui

*Department of Electrical Engineering, Indian Institute of Technology, Kharagpur, India*

Soumitro Banerjee<sup>a)</sup>

*Department of Electrical Engineering and Centre for Theoretical Studies, Indian Institute of Technology, Kharagpur, India*

(Received 7 May 2002; accepted 20 September 2002; published 19 November 2002)

We present the theory of border collision bifurcation for the special case where the state space is piecewise smooth, but two-dimensional in one side of the borderline, and one dimensional in the other side. This situation occurs in a class of switching circuits widely used in power electronic industry. We analyze this particular class of bifurcations in terms of the normal form, where the determinant of the Jacobian matrix at one side of the borderline is greater than unity in magnitude, and in the other side it is zero. © 2002 American Institute of Physics. [DOI: 10.1063/1.1521390]

**Border collision bifurcations occur in piecewise smooth (PWS) maps when a fixed point collides with a borderline separating two smooth regions. The discontinuous change in the Jacobian elements results in many atypical bifurcation phenomena, like a periodic orbit turning directly into a chaotic orbit, or multiple attractors coming into existence or going out of existence as the parameter is varied across some critical value, etc. So far the theory for border collision bifurcations has been developed for one- and two-dimensional PWS maps. Some results regarding the existence and stability of period-1 and period-2 orbits are also available for the general  $n$ -dimensional systems. However, recent research has shown that there may also be systems where the map is two dimensional in one side of the border, and one-dimensional in the other side. In the present paper we present various bifurcation phenomena that may occur under that condition.**

### I. INTRODUCTION

Following the pioneering work of Nusse and Yorke,<sup>1</sup> many researchers have investigated the phenomenon of border collision bifurcation that occur in piecewise smooth maps. In such maps, the state space (or phase space) is divided into two or more regions, and the dynamics are given by equations of the form

$$f(x,y;\rho) = \begin{cases} f_1(x,y;\rho) & \text{for } (x,y) \in R_1 \\ f_2(x,y;\rho) & \text{for } (x,y) \in R_2 \\ \vdots & \\ f_n(x,y;\rho) & \text{for } (x,y) \in R_n, \end{cases} \quad (1)$$

where  $R_1, R_2, \dots$ , are different smooth regions of the phase space, with *borderlines* dividing these regions. Much of the work on the dynamics of piecewise smooth maps<sup>4–6</sup> assumed

that (a) the function  $f$  is continuous across the borderlines, (b) the Jacobian of  $f$  is discontinuous across the borderlines, and (c) the Jacobian elements are finite.

Over the years, evidence has accumulated pointing towards occurrence of such maps in systems of practical importance. Most widely studied examples come from electrical engineering where power electronic circuits—which contain *switches* controlled by state feedback—routinely yield piecewise smooth maps under sampled-data modeling.<sup>2,3</sup> This has given impetus to the study of the dynamics of piecewise smooth maps. In piecewise smooth maps, a new class of bifurcation occur when a fixed point collides with the border—which causes a discontinuous change in the elements of the Jacobian matrix. Such bifurcations are in general called border collision bifurcations. In recent years, the border collision bifurcations occurring in one-dimensional and two-dimensional maps have been systematically investigated from the point of view of asymptotic behavior of orbits at the two sides of a border collision event.<sup>4,5</sup> In another line of development, the existence of period-one and period-two orbits have been investigated in the context of a general  $n$ -dimensional map.<sup>6</sup>

In the above work it was always assumed that the system dimension is the same over the whole of the state space. However, recent work on a class of power electronic circuits have shown that there may be systems where the state space dimension may be different at the two sides of the borderline. This has necessitated a thorough study of the bifurcations that may occur under such condition.

In Sec. II we first present the example of a system where the state space dimension changes from two to one across a borderline. In Sec. III the basic tools of this analysis—the normal form and its properties—are presented. We then proceed to analyze the various bifurcations that may occur in such systems. There are three possible situations that require separate treatment depending on the determinant of the system at one side of the border (that in the other side being zero):

(a) when the determinant is less than  $-1$ ,

<sup>a)</sup>Electronic mail: soumitro@ee.iitkgp.ernet.in

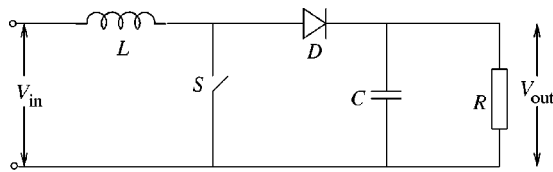


FIG. 1. Circuit diagram of the boost converter.

- (b) when the determinant is greater than +1,
- (c) when the determinant is between -1 and +1.

These three cases are treated in Secs. IV, V, and VI, respectively. Since a large number of cases depending on the parameters of the normal form need to be presented, we avoid the theorem–proof format that would make the paper very long. Instead, in each case we describe the mechanism of creation of attractors and the resulting bifurcations as a parameter is varied. Section VII contains the conclusions of this paper.

### II. A PRACTICAL EXAMPLE: THE DC–DC BOOST CONVERTER

The circuit shown in Fig. 1, called the boost converter, is widely used in industry to convert a lower dc voltage to a higher dc voltage. When the controlled switch  $S$  is on, the input voltage  $V_{in}$  is applied on the inductor and the inductor current rises. When it is off the inductor current falls, and the polarity of the inductor voltage reverses so that it adds to the input voltage. Therefore the output voltage  $V_{out}$  is greater than the input voltage  $V_{in}$ . The capacitor acts to smoothen the voltage across the load. The energy stored in the inductor during the *on* phase circulates through the load (the resistance  $R$ ) and the diode  $D$  during the off period. During the *on* period, the capacitor discharges through the load, thus maintaining a continuous load current flow.

The switch can be controlled by various control logics. Here we consider the current mode control where the switch turns off as the inductor current reaches a reference current

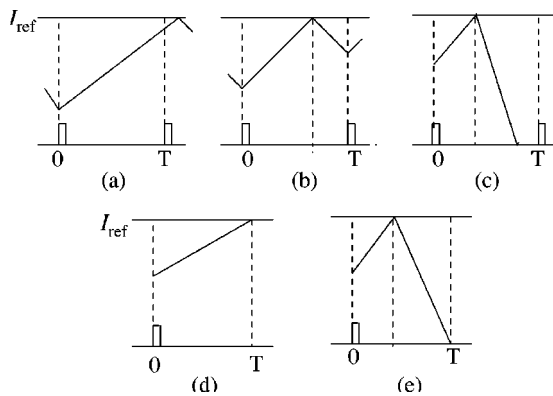


FIG. 2. Possible evolutions of the inductor current between two clock instants: (a) where the clock arrives before  $i$  reaches  $I_{ref}$ , (b) both on and off intervals are included in the clock period, (c) where  $i$  becomes zero for a part of the clock cycle. These three possibilities yield different functional forms of the map, separated by the borderline cases shown in (d) and (e): in situation (d) the clock arrives exactly when  $i$  reaches  $I_{ref}$ , and in situation (e)  $i$  becomes zero just at the end of the clock period.

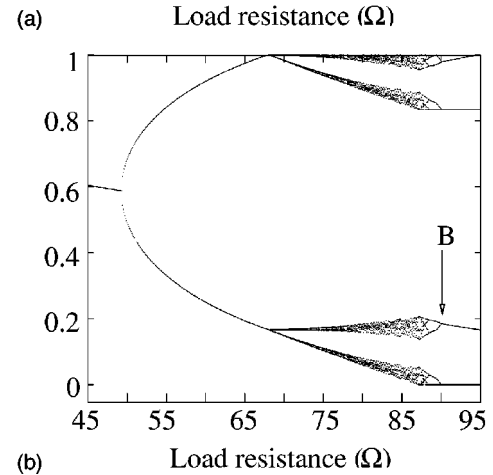
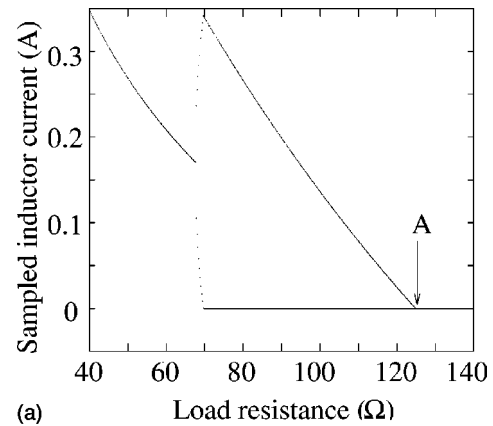


FIG. 3. Bifurcation diagrams of the boost converter. Left, with parameters  $L=0.2$  mH,  $C=47$   $\mu$ F,  $V_{in}=10$  V,  $T=33.33$   $\mu$ s,  $I_{ref}=1$  A, and load resistance  $R$  varied from  $40\Omega$  to  $140\Omega$ . Right, with the parameters  $L=0.4$  mH,  $C=22$   $\mu$ F,  $V_{in}=10$  V,  $T=33.33$   $\mu$ s,  $I_{ref}=1$  A and the load resistance varied from  $45\Omega$  to  $95\Omega$ .

$I_{ref}$ . A periodic clock signal generated separately is used to turn on the switch: after the switch turns off, it is turned on at the next clock pulse.

There are two main operating modes of the converter—the continuous conduction mode (CCM)<sup>7</sup> and the discontinuous conduction mode (DCM).<sup>8</sup> In CCM, the inductor current is always nonzero, and the switch and the diode are turned on and off in a complementary fashion. In DCM, the inductor current drops to zero before the next clock period begins and during this period both  $D$  and  $S$  do not conduct.

The inductor current  $i$  and the capacitor voltage  $v_c$  are the state variables of the system. We can construct the discrete-time model by observing the states in synchronism with the clock.<sup>9</sup> During the CCM mode of operation the map will be two dimensional, but during the DCM mode of operation it will be one-dimensional since the inductor current is always zero at the end of a clock period. Therefore the state space dimension changes from two to one when the converter shifts from CCM to DCM.<sup>10</sup>

Figure 2 shows that the discrete-time state space is divided into three regions, with three different equations giving the complete model of the system. Across the first borderline the state-space dimension remains the same but across the second borderline it changes from two to one. The functional

TABLE I. The possible types of fixed points of the normal form.

Type	Eigenvalues	Condition
<b>For <math>0 &lt; \delta &lt; 1</math></b>		
Regular attractor	$0 < \lambda_1 < 1, 0 < \lambda_2 < 1$	$2\sqrt{\delta} < \tau < (1 + \delta)$
Regular saddle	$0 < \lambda_1 < 1, \lambda_2 > 1$	$\tau > (1 + \delta)$
Flip attractor	$-1 < \lambda_1 < 0, -1 < \lambda_2 < 0$	$-(1 + \delta) < \tau < -2\sqrt{\delta}$
Flip saddle	$-1 < \lambda_1 < 0, \lambda_2 < -1$	$\tau < -(1 + \delta)$
Spiral attractor	$ \lambda_1 ,  \lambda_2  < 1$	eigenvalues complex
(a) Clockwise spiral		$0 < \tau < 2\sqrt{\delta}$
(b) Counter-clockwise spiral		$-2\sqrt{\delta} < \tau < 0$
<b>For <math>-1 &lt; \delta &lt; 0</math></b>		
Flip attractor	$-1 < \lambda_1 < 0, 0 < \lambda_2 < 1$	$-(1 + \delta) < \tau < (1 + \delta)$
Flip saddle	$\lambda_1 > 1, -1 < \lambda_2 < 0$	$\tau > 1 + \delta$
Flip saddle	$0 < \lambda_1 < 1, \lambda_2 < -1$	$\tau < -(1 + \delta)$
<b>For <math>\delta &gt; 1</math></b>		
Regular repeller	$\lambda_1 > 1, \lambda_2 > 1$	$2\sqrt{\delta} < \tau < (1 + \delta)$
Flip repeller	$\lambda_1 < -1, \lambda_2 < -1$	$-2\sqrt{\delta} > \tau > -(1 + \delta)$
Flip saddle	$-1 < \lambda_1 < 0, \lambda_2 < -1$	$\tau < -(1 + \delta)$
Regular saddle	$\lambda_1 > 1, 0 < \lambda_2 < 1$	$\tau > (1 + \delta)$
Spiral repeller	$ \lambda_1 ,  \lambda_2  > 1$	eigenvalues complex
(a) Clockwise spiral		$0 < \tau < 2\sqrt{\delta}$
(b) Counter-clockwise spiral		$-2\sqrt{\delta} < \tau < 0$
<b>For <math>\delta &lt; -1</math></b>		
Flip repeller	$\lambda_1 > 1, \lambda_2 < -1$	$(1 + \delta) < \tau < -(1 + \delta)$
Flip saddle	$0 < \lambda_1 < 1, \lambda_2 < -1$	$\tau < (1 + \delta)$
Flip saddle	$\lambda_1 > 1, -1 < \lambda_2 < 0$	$\tau < (1 + \delta)$
<b>For <math>\delta = 0</math></b>		
Regular attractor	$0 < \lambda_1 < 1, \lambda_2 = 0$	$0 < \tau < 1$
Regular saddle	$\lambda_1 > 1, \lambda_2 = 0$	$\tau > 1$
Flip saddle	$\lambda_1 < -1, \lambda_2 = 0$	$\tau < -1$
Flip attractor	$-1 < \lambda_1 < 0, \lambda_2 = 0$	$-1 < \tau < 0$

forms of the map and the borderlines can be found in Ref. 10.

Figure 3 presents two bifurcation diagrams where a fixed point collided with the second borderline (shown with arrows). Numerical determination of the eigenvalues show that at point *A*, the determinant in one side is  $-1.219$  and that in the other side is zero, and at point *B* the determinant in one side is  $-1.588$  and in the other side it is zero. Therefore, in such a system the determinant in one side of a border collision event may have magnitude *greater than one*—a possibility which has not been investigated so far.

Though this is the first studied case of a system with varying state space dimension, similar phenomena are expected to occur in many power electronic circuits and other types of systems. Hence the necessity of a theory for this special class of border collision bifurcations.

### III. THE NORMAL FORM AND ITS PROPERTIES

It has been shown earlier<sup>1,5</sup> that in the neighborhood of a border collision event, the nonlinear map can be approximated by a piecewise linear map (normal form) given by

$$g(x, y; \mu) = \begin{cases} \begin{pmatrix} \tau_L & 1 \\ -\delta_L & 0 \end{pmatrix} \begin{pmatrix} x \\ y \end{pmatrix} + \mu \begin{pmatrix} 1 \\ 0 \end{pmatrix} & \text{for } x \leq 0, \\ \begin{pmatrix} \tau_R & 1 \\ -\delta_R & 0 \end{pmatrix} \begin{pmatrix} x \\ y \end{pmatrix} + \mu \begin{pmatrix} 1 \\ 0 \end{pmatrix} & \text{for } x > 0, \end{cases} \quad (2)$$

where the state space is divided into two halves *L* and *R*.  $\tau_L$  and  $\delta_L$  are the trace and determinant of the Jacobian matrix in the left side of the borderline and  $\tau_R$  and  $\delta_R$  are these quantities in the right side, and  $\mu$  is the parameter.

Classifications of border collision bifurcations are generally done in terms of the parameters of the normal form (2),<sup>1,5,6</sup> namely  $\tau_L$ ,  $\delta_L$ ,  $\tau_R$ , and  $\delta_R$ . Presently we consider the condition  $\delta_R = 0$ , for which the locations of the fixed points at the two halves *L* and *R* are given by

$$L^* = \left( \frac{\mu}{1 - \tau_L + \delta_L}, \frac{-\delta_L \mu}{1 - \tau_L + \delta_L} \right), \quad (3)$$

$$R^* = \left( \frac{\mu}{1 - \tau_R}, 0 \right). \quad (4)$$

There are two basic categories of border collision bifurcations.<sup>5</sup>

- (1) Border collision pair bifurcation: A pair of fixed points are born on the border as the parameter is varied through  $\mu = 0$ . If the parameter is varied in the opposite direction, a pair of fixed points approach each other, and are annihilated as they collide on the border. Under this condition, (3) gives the location of  $L^*$  in the right half plane and (4) gives the position of  $R^*$  in the left half—meaning that the two fixed points do not exist. On the other side of  $\mu = 0$ , both fixed points exist—one in the

left half and the other in the right half of the state space. The condition for the occurrence of pair bifurcation can be obtained from the above consideration as

$$\tau_L > (1 + \delta_L) \quad \text{and} \quad \tau_R < 1 \tag{5}$$

when no fixed point exists for  $\mu < 0$  and a pair of fixed points exist for  $\mu > 0$ .

Similarly there will be another parameter range in which no fixed point exists for  $\mu > 0$  and two fixed points exist for  $\mu < 0$ . Its condition of occurrence is found to be

$$\tau_L < (1 + \delta_L) \quad \text{and} \quad \tau_R > 1. \tag{6}$$

- (2) Border crossing bifurcation: If (5) or (6) are not satisfied, a fixed point crosses the borderline as  $\mu$  is varied from a negative value to a positive value. Bifurcation occurs due to the change of the character of the fixed point as it crosses the border.

The stability of the fixed points in the above two cases are governed by the eigenvalues which, for the locally linearized map, are

$$\lambda_1 = \frac{1}{2}(\tau + \sqrt{\tau^2 - 4\delta}), \quad \lambda_2 = \frac{1}{2}(\tau - \sqrt{\tau^2 - 4\delta}), \tag{7}$$

where  $\tau$  and  $\delta$  refer to the trace and determinant of the eigenvalue of the fixed point in question.

We can categorize fixed points depending on the nature of orbits in the neighborhood of the fixed points. The various types of fixed points for the normal form map (2) are defined in Table I.

In working out the character of the attractors, we make use of the following properties of map (2). First, any point on the  $y$ -axis maps to a point on the  $x$ -axis. The forward iterates of a point on the unstable manifold will remain on the unstable manifold. As an unstable manifold crosses the border, i.e., the  $y$ -axis, one linear map changes to another linear map. So the slope of the unstable manifold in two sides of the  $x$ -axis will be different unless the map is smooth, i.e.,  $\tau_L = \tau_R$  and  $\delta_L = \delta_R$ . Thus for a piecewise smooth map the unstable manifold will fold at every intersection with the  $x$ -axis. Moreover, the images of every fold point will also be a fold point. In case of stable manifold the same argument applies for the inverse map, and we conclude that the stable manifold will fold at every intersection with the  $y$ -axis and the preimage of every fold point will be a fold point.

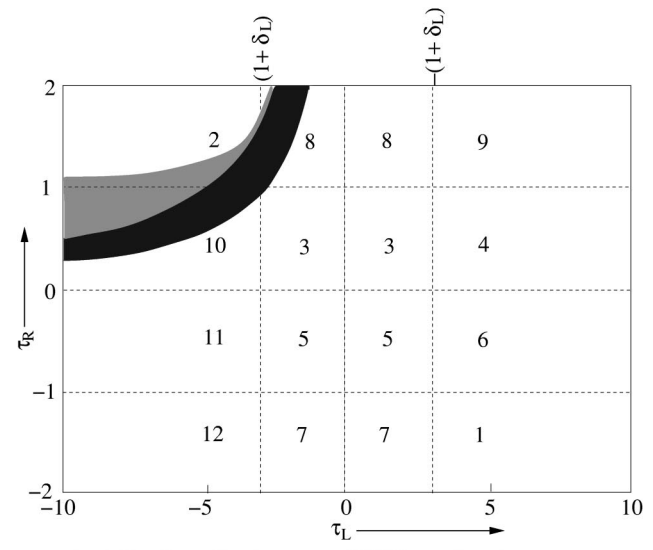
Second, as the system is linear in each side, period-2 or higher period fixed points cannot exist with all points in  $L$  or all points in  $R$  side. Therefore, if a period-2 orbit exists, it must have one point in  $L$  and another in  $R$ . The condition for existence of such an orbit is

$$\frac{-\mu(1 + \tau_R)}{\tau_L \tau_R - (1 + \delta_L)} < 0 \quad \text{and} \quad \frac{-\mu(1 + \tau_L + \delta_L)}{\tau_L \tau_R - (1 + \delta_L)} > 0. \tag{8}$$

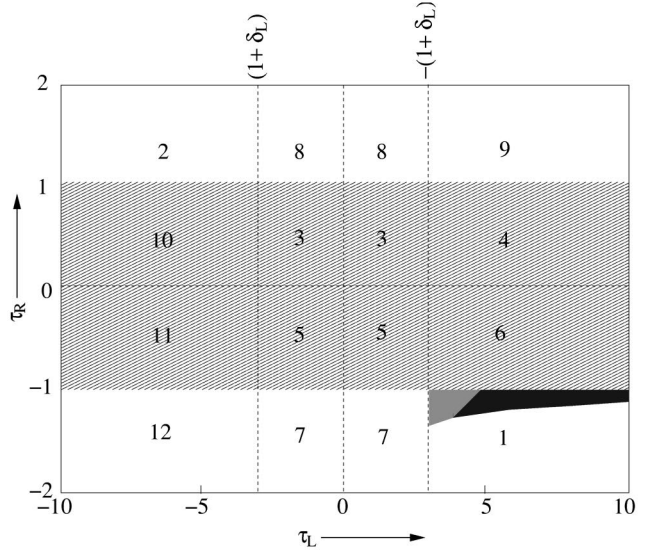
The eigenvalues of the period-2 orbit are  $(\tau_R \tau_L - \delta_L)$  and 0. The period-2 orbit will be stable if  $-1 < \tau_R \tau_L - \delta_L < +1$ . From this the condition for the stability of the period-2 orbit is obtained as

$$1 - \tau_L \tau_R + \delta_L > 0, \tag{9}$$

$$1 + \tau_L \tau_R - \delta_L > 0. \tag{10}$$



(a) Legend:   
 - Region of existence of HPO or chaotic attractor (shaded)   
 - Region of existence of period-2 orbit (black)   
 - No attractor (white)



(b) Legend:   
 - Region of existence of period-1 orbit (hatched)   
 - Region of existence of period-2 orbit (shaded)   
 - Region of existence of HPO or chaotic attractor (black)   
 - No attractor (white)

FIG. 4. Schematic diagram of the parameter space partitioning for  $\delta_L < -1, \delta_R = 0$ ; (a) for  $\mu < 0$  and (b) for  $\mu > 0$ . The dynamics in the numbered regions are discussed in the text.

**IV. THE CLASSIFICATION FOR  $\delta_L < -1$  AND  $\delta_R = 0$**

We make a primary division of the parameter space depending on the character of fixed points at the two regions  $L$  and  $R$ . Since the fixed point in  $L$  can be of three types and that in  $R$  can be of four types, the parameter space can be partitioned into 12 regions where different types of border collision bifurcations are expected to occur. These are shown in Fig. 4. We now discuss briefly the phenomenology that occur in each region.

**A. Border collision pair bifurcation**

If (5) and (6) are satisfied, there is no fixed point and hence no attracting orbit for one side of  $\mu = 0$ , and in the

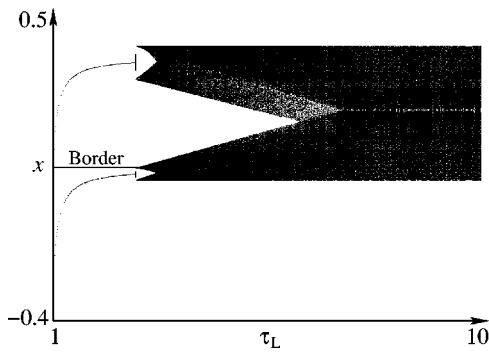


FIG. 5. The bifurcation diagram for Region 1 in negative determinant case with  $\tau_L$  as parameter and  $\tau_R = -1.1$ ,  $\delta_L = -2$ ,  $\delta_R = 0$ , and  $\mu = 0.4$ .

other side of  $\mu = 0$  two fixed points exist. Here we explore the character of the stable orbit when fixed points exist.

Region 1:  $\tau_L > -(1 + \delta_L)$  and  $\tau_R < -1$

Two fixed points exist for  $\mu > 0$  in  $L$  and  $R$ , and both are flip saddles. Due to the flip property of the fixed points, iterates in  $L$  move to  $R$  and iterates in  $R$  move to  $L$ . The period-2 orbit exists if (8) is satisfied, and is stable if (9) and (10) are satisfied. When (10) is violated the attractor becomes chaotic. The transition from the period-2 orbit to the chaotic attractor can be seen in the bifurcation diagram drawn with  $\tau_L$  as the parameter (Fig. 5). It is seen that at a critical value of  $\tau_L$ , a period-doubling occurs and subsequently the resulting orbit hits the borderline. Therefore the transition from periodic to chaotic orbit occurs through a border collision.

The structure of the chaotic attractor at  $\tau_L = 6.0$  is shown in Fig. 6. The attractor lies on the unstable manifold of  $R^*$ . Any point in  $R$  maps to the  $x$ -axis and moves away from  $R^*$ . Since the expression of the map is different at the two sides of the origin  $O$ , the extremities of the attractor are formed by forward iterates of the origin as:  $O \mapsto B$ ,  $B \mapsto A$ ,  $A \mapsto C$ ,  $C \mapsto D$ ,  $D \mapsto E$ —creating a two-piece chaotic attractor. With the change in parameter the two pieces join to form a single piece attractor.

The basin boundary is formed by the stable manifold of  $L^*$  which folds at the intersections with the  $y$ -axis. At a critical parameter value a boundary crisis occurs (when point

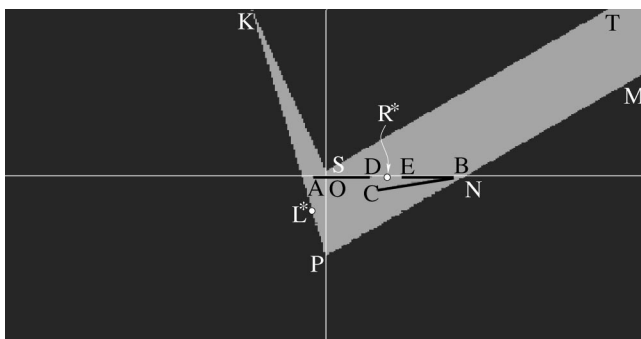


FIG. 6. The basin boundary and the chaotic attractor for Region 1 in negative determinant case with  $\tau_L = 6$ ,  $\delta_L = -2$ ,  $\tau_R = -1.1$ ,  $\delta_R = 0$ , and  $\mu = 0.4$ .

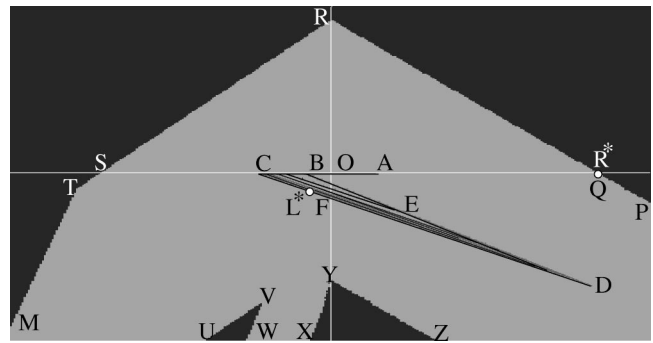


FIG. 7. The basin boundary and the chaotic attractor for Region 2 in negative determinant case with  $\tau_L = -4.0$ ,  $\delta_L = -3$ ,  $\tau_R = 1.1$ ,  $\delta_R = 0$ , and  $\mu = -0.1$ .

$B$  touches the basin boundary at  $N$ ) and the attractor is annihilated.

Therefore in this region of the parameter space, one can have the birth of a period-2 orbit, a chaotic orbit, or an unstable chaotic orbit as  $\mu$  is varied through zero.

Region 2:  $\tau_L < (1 + \delta_L)$  and  $\tau_R > 1$

For  $\mu < 0$  two fixed points exist—a flip saddle in  $L$  and a regular saddle in  $R$ . The phenomenology is similar to that in Region-1: the period-2 orbit is stable if (9) and (10) are satisfied, and when (10) is violated the attractor becomes chaotic, through period doubling followed by border collision.

The structure of the chaotic attractor at  $\tau_L = -4.0$  is shown in Fig. 7. The attractor is formed by the unstable manifold of  $L^*$  which is located on the attractor. In the attractor  $OB \mapsto BE$ ,  $FC \mapsto CD$ ,  $FD \mapsto CA$ ,  $BC \mapsto ED$ , thus  $A$ ,  $C$ , and  $D$  become the extremities. The basin boundary is formed by the stable manifold of  $R^*$  which is a saddle. At a critical parameter value, boundary crisis may occur, annihilating the attractor. Therefore in this region also, one can have the birth of a period-2 orbit, a chaotic orbit or an unstable chaotic orbit as  $\mu$  is varied through zero.

Region 3:  $(1 + \delta_L) < \tau_L < -(1 + \delta_L)$  and  $0 < \tau_R < 1$

For  $\mu > 0$  there is a flip repeller in  $L$  and a regular attractor in  $R$ . All initial conditions in  $L$  flip to  $R$ . All initial conditions in the  $R$  side map to points on the  $x$ -axis and then converge onto  $R^*$ . So we get a stable period-1 attractor for  $\mu > 0$ .

Region 4:  $\tau_L > -(1 + \delta_L)$  and  $0 < \tau_R < 1$

For  $\mu > 0$ ,  $L^*$  is a flip saddle and  $R^*$  is a regular attractor. This is like a saddle-node bifurcation and we get a stable period one attractor for  $\mu > 0$ .

Region 5:  $(1 + \delta_L) < \tau_L < -(1 + \delta_L)$  and  $-1 < \tau_R < 0$

For  $\mu > 0$ , there is a flip repeller in the  $L$  side and a flip attractor in the  $R$  side. Initial conditions in  $L$  will be repelled to the  $R$  side, and the initial conditions in the  $R$  side will converge on  $R^*$ . So a stable period-1 attractor exists for  $\mu > 0$ .

Region 6:  $\tau_L > -(1 + \delta_L)$  and  $-1 < \tau_R < 0$

For  $\mu > 0$ ,  $L^*$  is a flip saddle and  $R^*$  is a flip attractor. This is also like a saddle-node bifurcation and we get a period-1 attractor for  $\mu > 0$ .

Therefore in the regions 3, 4, 5, and 6 there is a birth of

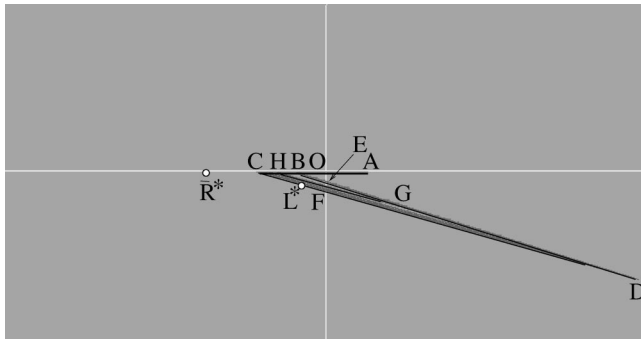


FIG. 8. The chaotic attractor of Region 10 in negative determinant case, for  $\tau_L = -5$ ,  $\delta_L = -3$ ,  $\tau_R = 0.9$ ,  $\delta_R = 0$ , and  $\mu = -0.1$ .

a period-1 attractor at  $\mu = 0$  as the parameter is varied from a negative value to a positive value.

Region 7:  $(1 + \delta_L) < \tau_L < -(1 + \delta_L)$  and  $\tau_R < -1$

For  $\mu < 0$  there is a flip repeller in the  $L$  side and a flip saddle in the  $R$  side. The initial conditions in the  $R$  side diverge due to the repelling action of  $L^*$ . The initial conditions in the  $R$  side flip to  $L$ , and then diverge to infinity. Therefore no attractor can exist for any value of  $\mu$ .

**B. Border crossing bifurcation**

In a border crossing bifurcation, a fixed point crosses the border as  $\mu$  is varied through zero, and may become a different kind of fixed point. When (3) shows that the fixed point is in  $L$ , the dynamics of points in the  $L$  side are guided by the character of the fixed point  $L^*$ . For that value of the

parameter, if we calculate the location of the fixed point  $R^*$  from (4), we find that it is also located in the  $L$  side, and therefore actually does not exist. However, such a nonexistent fixed point has significant influence on the system dynamics because the trajectories of points in  $R$  side are guided by its location and character. Such a fixed point will be called a *virtual fixed point* and will be denoted by the overbar sign  $\bar{R}^*$ . Similarly, when  $R^*$  exists,  $\bar{L}^*$  becomes a virtual fixed point.

Region 8:  $(1 + \delta_L) < \tau_L < -(1 + \delta_L)$  and  $\tau_R > 1$   
(Regular saddle changes to flip repeller)

For  $\mu < 0$ ,  $R^*$  exists and is a regular saddle, while  $\bar{L}^*$  is a flip repeller. For  $\mu < 0$ , initial conditions in  $R$  converge on to the unstable manifold. The segment of the unstable manifold to the right of  $R^*$  goes to infinity, and the segment to the left goes towards  $L$ . In side  $L$ , all points map to  $R$  because of the flip property of  $\bar{L}^*$ . A period-2 orbit can exist, with a point each in  $L$  and  $R$ , if (9) and (10) are satisfied. When (10) is violated, a period doubling occurs followed by a border collision, creating a chaotic orbit. Both the period-2 attractor and the chaotic attractor are located on the unstable manifold of  $R^*$ . The basin boundary is formed by the stable manifold of  $R^*$ . At a critical parameter value the chaotic attractor is annihilated due to boundary crisis.

For  $\mu > 0$ ,  $L^*$  is a flip repeller and  $\bar{R}^*$  is a regular saddle. The action of the flip repeller  $L^*$  causes all initial conditions in  $L$  to flip to the  $R$  side in some iterate, and then the action of  $\bar{R}^*$  makes it diverge to infinity along its unstable direction, i.e., the  $x$ -axis.

TABLE II. The nature of the fixed points and the type of bifurcations for  $\delta_L < -1$  and  $\delta_R = 0$ .

Region	$\mu < 0$	$\mu > 0$	Type of bifurcation
Border collision pair bifurcations			
Region 1: $\tau_R < -1$ , $\tau_L > -(1 + \delta_L)$	No fixed point	$L^*$ -flip saddle $R^*$ -flip saddle	Birth of period-2 attractor, chaotic attractor, or unstable chaotic orbit for $\mu > 0$
Region 2: $\tau_R > 1$ , $\tau_L < (1 + \delta_L)$	$L^*$ -flip saddle $R^*$ -regular saddle	No fixed point	Birth of a period-2 attractor, or a chaotic attractor, or an unstable chaotic orbit for $\mu < 0$
Region 3: $0 < \tau_R < 1$ , $(1 + \delta_L) < \tau_L < -(1 + \delta_L)$	No fixed point	$L^*$ -flip repeller $R^*$ -regular attractor	Birth of a period-1 attractor for $\mu > 0$
Region 4: $0 < \tau_R < 1$ , $\tau_L > -(1 + \delta_L)$	No fixed point	$L^*$ -flip saddle $R^*$ -regular attractor	Birth of a period-1 attractor for $\mu > 0$
Region 5: $-1 < \tau_R < 0$ , $(1 + \delta_L) < \tau_L < -(1 + \delta_L)$	No fixed point	$L^*$ -flip repeller $R^*$ -flip attractor	Birth of a period-1 attractor for $\mu > 0$
Region 6: $-1 < \tau_R < 0$ , $\tau_L > -(1 + \delta_L)$	No fixed point	$L^*$ -flip saddle $R^*$ -flip attractor	Birth of a period-1 attractor for $\mu > 0$
Region 7: $\tau_R < -1$ , $(1 + \delta_L) < \tau_L < -(1 + \delta_L)$	No fixed point	$L^*$ -flip repeller $R^*$ -flip saddle	No attractor for any value of $\mu$
Border crossing bifurcations			
Region 8: $\tau_R > 1$ , $(1 + \delta_L) < \tau_L < -(1 + \delta_L)$	$R^*$ -regular saddle	$L^*$ -flip repeller	Period-2, or chaotic attractor, or no attractor for $\mu < 0$ and no attractor for $\mu > 0$
Region 9: $\tau_R > 1$ , $\tau_L > -(1 + \delta_L)$	$R^*$ -regular saddle	$L^*$ -flip saddle	No attractor for any value of $\mu$
Region 10: $0 < \tau_R < 1$ , $\tau_L < (1 + \delta_L)$	$L^*$ -flip saddle	$R^*$ -regular attractor	Period-2, or chaotic attractor or no attractor for $\mu < 0$ and period-1 for $\mu > 0$
Region 11: $-1 < \tau_R < 0$ , $\tau_L < (1 + \delta_L)$	$L^*$ -flip saddle	$R^*$ -flip attractor	No attractor for $\mu < 0$ , period-1 for $\mu > 0$
Region 12: $\tau_R < -1$ , $\tau_L < (1 + \delta_L)$	$L^*$ -flip saddle	$R^*$ -flip saddle	No attractor for any value of $\mu$

Therefore in this region, if  $\mu$  is increased from a negative value, the attractor (either period-2 or chaotic) vanishes at  $\mu=0$ .

Region 9:  $\tau_L > -(1 + \delta_L)$  and  $\tau_R > 1$   
(Regular saddle changes to flip saddle)

For  $\mu < 0$ ,  $R^*$  is a regular saddle and  $\bar{L}^*$  is a flip saddle. The initial conditions in the  $R$  side diverge along the unstable manifold of  $R^*$ . The initial conditions in the  $L$  side flip to the  $R$  side due to the action of  $\bar{L}^*$  and then move outwards along the unstable direction of  $R^*$ . So no attractor exists for  $\mu < 0$ .

For  $\mu > 0$ ,  $L^*$  is a flip saddle and  $\bar{R}^*$  is a regular saddle. The flip property of  $L^*$  is along the stable direction, and the unstable direction has a positive eigenvalue. Therefore, the initial conditions which are to the left of  $L^*$  will gradually diverge along the unstable direction of  $L^*$  and those which are to the right of  $L^*$  will gradually move to the  $R$  side. Points in  $R$  diverge along the  $x$ -axis, which is the unstable direction of  $\bar{R}^*$ . So no attractor exists for  $\mu > 0$ .

Thus in this region of the parameter space, there is no stable attractor for any value of  $\mu$ .

Region 10:  $\tau_L < (1 + \delta_L)$  and  $0 < \tau_R < 1$   
(Flip saddle changes to regular attractor)

For  $\mu < 0$ ,  $L^*$  is a flip saddle. Therefore the initial conditions in the  $L$  side will flip along the unstable manifold of  $L^*$  and will move over to the  $R$  side in subsequent iterates. Iterates in  $R$  will be guided by  $\bar{R}^*$  which is a regular attractor, and so initial conditions in  $R$  will move to the  $L$  side.

Since points in  $L$  move to  $R$  and points in  $R$  move to  $L$ , there is a possibility of a period-2 orbit. If (8) is satisfied, a period-2 orbit exists, and if (9) and (10) are satisfied, it is stable. As  $\tau_L$  is reduced, condition (9) is approached and the distance between the period two fixed points gradually increases and finally becomes infinite and no attractor exists after that.

When  $\tau_L$  is increased, at a point (10) is violated, and the period-2 orbit goes through period doubling after which one of the branches hits the border, giving rise to a chaotic attractor in a phenomenology similar to that in Fig. 5.

Both the period-2 orbit and the chaotic attractor must lie on the unstable manifold of  $L^*$ . The chaotic attractor obtained following the instability of the period-2 orbit is shown in Fig. 8. The extremities of the attractor are formed by forward iterates of the intersections with  $y$ -axis:  $O \mapsto B$ ,  $B \mapsto G$ ,  $F \mapsto C$ ,  $C \mapsto D$ ,  $E \mapsto H$ , and  $D \mapsto A$ . The basin of attraction spans the whole state space.

For  $\mu > 0$ ,  $\bar{L}^*$  is a flip saddle and  $R^*$  is a regular attractor. All initial conditions in the  $R$  side converge on to  $R^*$  and all initial condition in the  $L$  side flip to the  $R$  side due to the action of  $\bar{L}^*$  and finally converge on to  $R^*$ . So we get a stable period-one attractor for  $\mu > 0$ .

Therefore in this region of the parameter space as  $\mu$  is decreased from a positive value to a negative value, one has a transition from period-1 to either period-2 orbit [if (9) and (10) are satisfied] or chaotic orbit [if (10) is violated] or no attractor [if (9) is violated].

Note that in the boost converter example, the bifurcation points  $A$  and  $B$  in Fig. 3 fall under this category. The calcu-

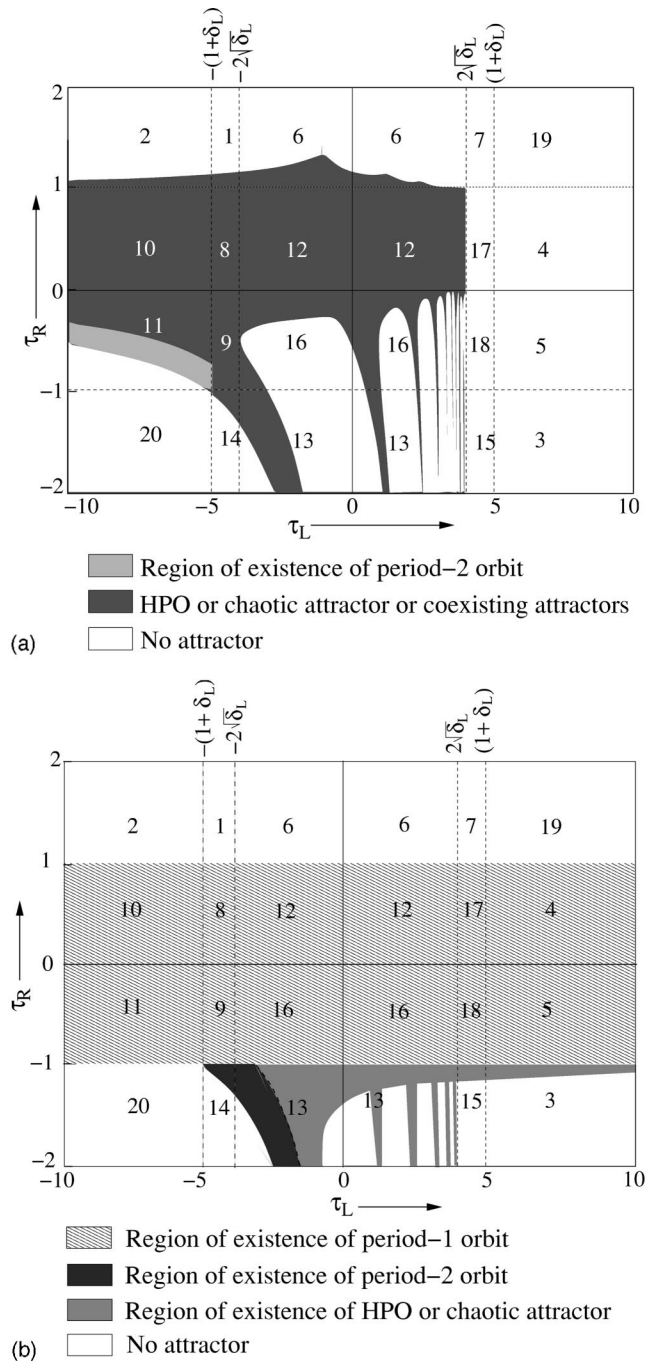


FIG. 9. Schematic diagram of the parameter space partitioning for  $\delta_L > 1$ ,  $\delta_R = 0$  showing existence of attractors, (a) for  $\mu < 0$ , (b) for  $\mu > 0$ .

lated values of the normal form parameters are as follows. For point  $A$ ,  $\tau_L = -0.2526$ ,  $\delta_L = -1.219$ ,  $\tau_R = 0.9838$ , and  $\delta_R = 0$ . For point  $B$ ,  $\tau_L = -1.027$ ,  $\delta_L = -1.588$ ,  $\tau_R = 0.7196$ , and  $\delta_R = 0$ . Since (9) and (10) are satisfied, we see period doubling phenomenon due to border collision.

Region 11:  $\tau_L < (1 + \delta_L)$  and  $-1 < \tau_R < 0$   
(Flip saddle changes to flip attractor)

For  $\mu < 0$ ,  $L^*$  is a flip saddle and  $\bar{R}^*$  is a flip attractor. Initial conditions in the  $R$  side flip to the other side of  $\bar{R}^*$  and land in the  $L$  side. Points in  $L$  move outwards along the unstable eigenvector of  $L^*$ . Since (9) and (10) are not satis-

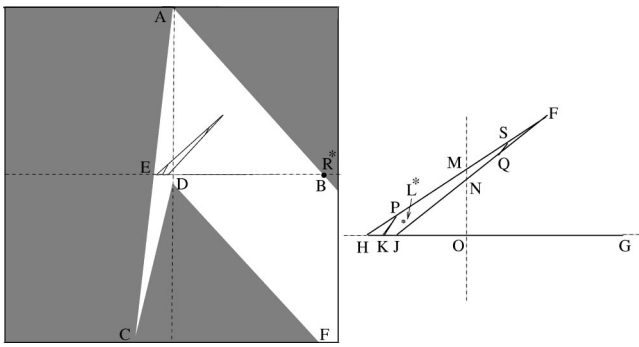


FIG. 10. The basin boundary and the chaotic attractor for Region 1 in positive determinant case with  $\tau_L = -4.5$ ,  $\delta_L = 4$ ,  $\tau_R = 1.1$ ,  $\delta_R = 0$ , and  $\mu = -0.2$ .

fied, period-2 orbit is not stable. No other attractor can exist for  $\mu < 0$ .

For  $\mu > 0$   $R^*$  is a flip attractor and  $\bar{L}^*$  is a flip saddle. All initial conditions in the  $R$  side converge on to  $R^*$ . The initial conditions in the  $L$  side move to the  $R$  side due to the action of  $\bar{L}^*$  and finally converge on to  $R^*$ . So we get a stable period one attractor for  $\mu > 0$ .

Region 12:  $\tau_L < (1 + \delta_L)$  and  $\tau_R < -1$   
(Flip saddle remains flip saddle)

For  $\mu < 0$ ,  $L^*$  and  $\bar{R}^*$  are both flip saddles. The initial conditions in the  $L$  side flip along the unstable direction of  $L^*$  and move to the  $R$  side. Points in the  $R$  side come to the  $L$  side due to the action of  $\bar{R}^*$  and flip along the unstable direction of  $L^*$ . As the fixed point of the second iterate is a saddle, the points will diverge to infinity along its unstable direction. So no attractor exists for any value of  $\mu < 0$ .

For  $\mu > 0$ , the same phenomenon occurs, and no attractor can exist.

The bifurcation phenomena for  $\delta_L < -1$  and  $\delta_R = 0$  are summarized in Table II.

### V. THE PARAMETER SPACE PARTITIONING FOR $\delta_L > 1$ AND $\delta_R = 0$

When the determinant is positive, there can be five types of fixed points in the left side and 4 types of fixed points in the right side. Therefore the parameter space can be divided into 20 regions depending on the type of fixed points—as shown in Fig. 9.

#### A. Border collision pair bifurcation

Since no fixed point and hence no attractor exists in one side of  $\mu = 0$ , we discuss only the character of the attractor when fixed points exist.

Region 1:  $-(1 + \delta_L) < \tau_L < -2\sqrt{\delta_L}$  and  $\tau_R > 1$

For  $\mu < 0$ ,  $L^*$  is a flip repeller and  $R^*$  is a regular saddle. The shape of the chaotic attractor existing in this region is shown in Fig. 10.

$B$  is location of  $R^*$ .  $FDCEAB$  is the basin boundary formed by the stable manifold of  $R^*$ . Any point on line  $AB$  maps to point  $B$ . So from the map we get the slope of the line  $AB$  as  $-\tau_R$ . In the basin boundary  $DC \mapsto EA$ ,  $DF \mapsto E$ ,  $CA \mapsto AB$  and  $AB \mapsto B$ .

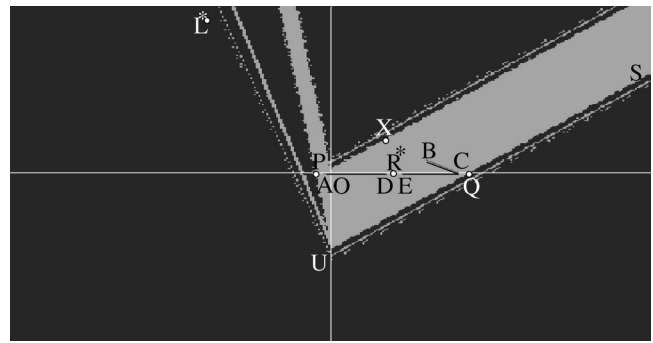


FIG. 11. Basin boundary and chaotic attractor for Region 3 in positive determinant case with  $\tau_L = 5.1$ ,  $\tau_R = -1.05$ ,  $\delta_L = 4$ ,  $\delta_R = 0$ , and  $\mu = 0.4$ .

The chaotic attractor lies on the unstable manifold of  $R^*$ . Any point in side  $R$ , lying to the left of  $AB$  maps to the  $x$ -axis, and then moves along this unstable manifold towards side  $L$ . Since the origin  $O \mapsto H$ , and since the map changes across the border, the unstable manifold experiences a fold at  $H$ . The rest of the attractor is composed by line segments obtained by the forward iterates of  $OH$ , as  $OH \mapsto HF$ ,  $HM \mapsto FJ$ ,  $MF \mapsto JG$ ,  $OJ \mapsto HP$ ,  $KP \mapsto SQ$ ,  $HK \mapsto FS$ , thus forming the attractor.

The repeller  $L^*$  lies within the attractor, and all points close to it move outwards, and converge on the attractor since  $L^*$  is enclosed from all sides by the attractor.

As the parameters are varied within Region 1, the shape of the attractor and the basin boundary undergo quantitative changes. At some combination of parameter values, they come in contact, and the orbit becomes unstable at boundary crisis.

Region 2:  $\tau_L < -(1 + \delta_L)$  and  $\tau_R > 1$

For  $\mu < 0$ ,  $L^*$  is a flip saddle and  $R^*$  is a regular saddle. In this parameter range we have chaotic attractor for  $\mu < 0$ , and the phenomenology is similar to that in Region 1.  $L^*$  is enclosed within the attractor formed by the unstable manifold of  $R^*$ . The basin boundary is formed by the stable manifold of  $R^*$ . When the origin maps to a point on the basin boundary, a boundary crisis occurs.

Region 3:  $\tau_L > (1 + \delta_L)$  and  $\tau_R < -1$

For  $\mu > 0$ ,  $L^*$  is a regular saddle and  $R^*$  is a flip saddle. A chaotic attractor is organized by the flip saddle  $R^*$ , whose

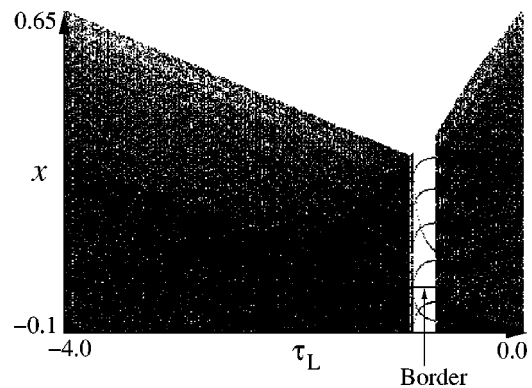


FIG. 12. The bifurcation diagram for Region 6 with  $\tau_L$  as parameter (varied from  $-4$  to  $0$ ) with  $\tau_R = 1.1$ ,  $\delta_L = 4$ ,  $\delta_R = 0$ , and  $\mu = -0.1$ .

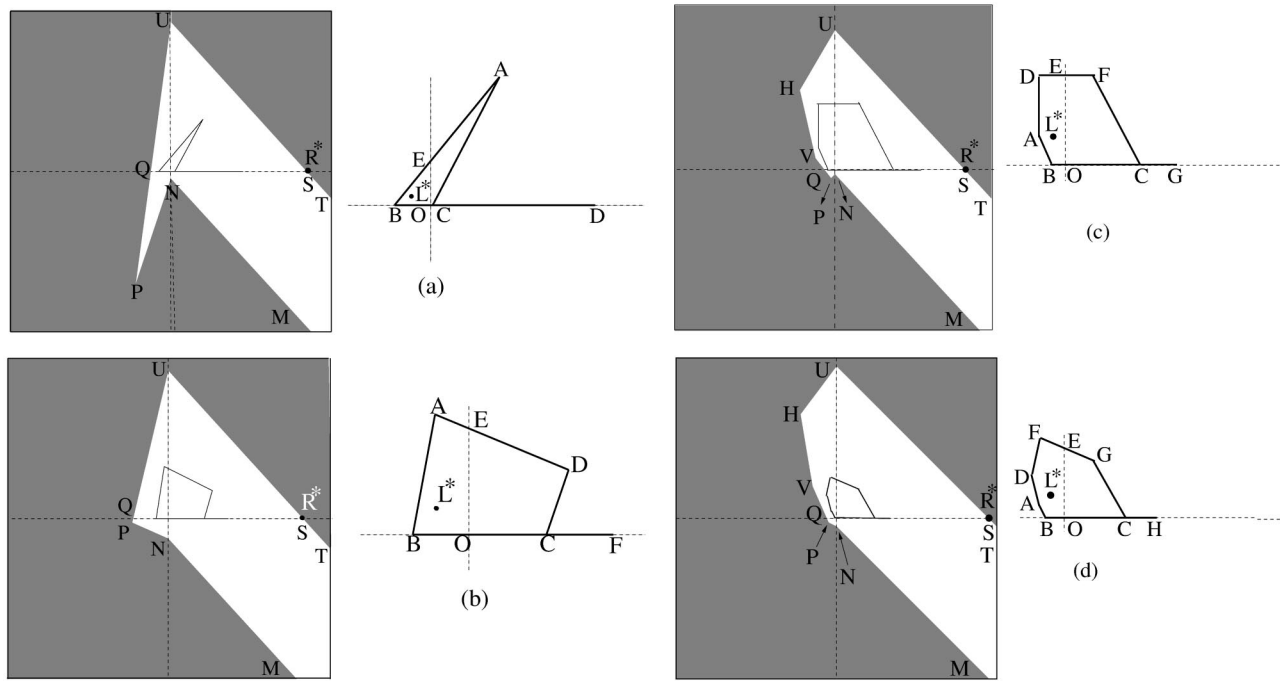


FIG. 13. The chaotic attractors for different combinations of the parameters for Region 6 in positive determinant case: (a)  $\tau_L = -3.5$ ,  $\delta_L = 4$ ,  $\tau_R = 1.1$ ,  $\delta_R = 0$ , and  $\mu = -0.1$ . (b)  $\tau_L = -0.5$ ,  $\delta_L = 4$ ,  $\tau_R = 1.1$ ,  $\delta_R = 0$ , and  $\mu = -0.1$ . (c)  $\tau_L = 2.0$ ,  $\delta_L = 4$ ,  $\tau_R = 1.04$ ,  $\delta_R = 0$ , and  $\mu = -0.1$  (d)  $\tau_L = 2.7$ ,  $\delta_L = 4$ ,  $\tau_R = 1.01$ ,  $\delta_R = 0$ , and  $\mu = -0.1$ .

unstable eigenvector lies along the  $x$ -axis (Fig. 11). Any initial condition in  $R$  maps to the  $x$ -axis and diverges away from  $R^*$ . As it crosses the origin, the map changes and the further iterates fall away from the  $x$ -axis. By the action of  $L^*$ , the iterates map back to  $R$ . The extremities of the attractor are formed by forward iterates of the origin:  $O \mapsto C$ ,  $C \mapsto A$ ,  $A \mapsto B$ ,  $B \mapsto D$  and  $D \mapsto E$ .

Basin boundary exists and it is formed by the stable manifold of the third iterate fixed point, which is a saddle.  $P$ ,  $Q$ , and  $X$  are the locations of the fixed points of the third iterate. The stable manifold through  $Q$  is along  $SU$ , and the unstable manifold is along the  $x$ -axis. The stable manifold folds at  $U$  and intersects with the unstable manifold as it crosses the  $x$ -axis. One intersection between stable and unstable manifold implies an infinite number of intersections, leading to a fractal structure of the basin boundary.

At a critical combination of parameter values, the attractor contacts the basin boundary. No attractor exists after this boundary crisis.

Regions 4 and 5:  $\tau_L > (1 + \delta_L)$  and  $-1 < \tau_R < 1$

For  $\mu > 0$ , one fixed point is regular saddle at the  $L$  side and the other is an attractor in the  $R$  side. If  $0 < \tau_R < 1$  then  $R^*$  is a regular attractor and if  $-1 < \tau_R < 0$  then it is a flip attractor. This is like a saddle-node bifurcation.

For  $\mu < 0$  all points diverge to infinity, and for  $\mu > 0$  all points are attracted to  $R^*$ , thus giving a period-1 attractor.

Region 6:  $-2\sqrt{\delta_L} < \tau_L < 2\sqrt{\delta_L}$  and  $\tau_R > 1$

For  $\mu < 0$ ,  $L^*$  is a repelling spiral and  $R^*$  is a regular saddle. We get high periodic orbits or chaotic attractor for  $\mu < 0$ . The bifurcation diagram with  $\tau_L$  as the parameter (and  $\mu$  fixed) is shown in Fig. 12. It shows that the transition from chaotic orbit to high periodic orbit occurs due to border col-

lision pair bifurcation in the seventh iterate (one point of the periodic orbit lies on the border at the bifurcation).

For different values of the parameter we get chaotic attractors of different shapes as shown in Fig. 13. The basin boundary is formed by the stable manifold of  $R^*$ .  $R^*$  is located at  $S$  and the stable eigenvector with eigenvalue zero is  $UT$ . Therefore  $UT \mapsto S$ . The stable manifold folds at the  $y$ -axis at  $U$  and at all preiterates of  $U$ , forming the basin boundary.

The attractor is formed in the following manner. In Fig. 13(a) the origin  $O \mapsto B$ ,  $B \mapsto A$ ,  $A \mapsto D$ , and  $E \mapsto C$ . These form the extremities of the attractor. The segments  $OB \mapsto BA$ ,  $BE \mapsto AC$  and  $EA \mapsto CD$ . As  $\tau_L$  is increased, the point  $A$  moves to the  $L$  side, and so the structure of the attractor changes, as shown in Fig. 13(b). In this attractor the origin  $O \mapsto B$ ,  $B \mapsto A$ ,  $A \mapsto D$ ,  $D \mapsto F$ ,  $E \mapsto C$ ,  $F \mapsto$  a point on  $CF$  and  $C \mapsto$  a point on  $OC$ . So the segments  $BA \mapsto AD$ ,  $AE \mapsto DC$ ,  $ED \mapsto CF$  and  $OB \mapsto BA$ .  $FC \mapsto$  a segment on  $OF$  and further iterate of this segment  $\mapsto OC$ . As  $\tau_L$  is increased further, the point  $D$  moves to the  $L$  side, and the attractor assumes a pentagonal structure as shown in Fig. 13(c) where  $O \mapsto B$ ,  $B \mapsto A$ ,  $A \mapsto D$ ,  $D \mapsto F$ ,  $F \mapsto G$ ,  $E \mapsto C$ . Likewise, with further increase in  $\tau_L$ , the attractor gets one additional segment. In Fig. 13(d)  $O \mapsto B$ ,  $B \mapsto A$ ,  $A \mapsto D$ ,  $D \mapsto F$ ,  $F \mapsto G$ ,  $G \mapsto H$ ,  $E \mapsto C$ ,  $H \mapsto$  a point on  $CH$  and  $C \mapsto$  a point on  $OC$ .  $L^*$  lies within the attractor.

As any part of the attractor touches the basin boundary, the attractor becomes unstable at a boundary crisis. Since for different parameter values we get chaotic attractors of different shapes, the condition of occurrence of the boundary crisis

changes discretely as additional segments are added in the attractor and/or the basin boundary. This gives the particular structure of the parameter space region where attractors exist as seen in Fig. 9(a) (see Region 6).

Region 7:  $2\sqrt{\delta_L} < \tau_L < (1 + \delta_L)$  and  $\tau_R > 1$

A regular repeller and a regular saddle are born in the  $L$  and  $R$  side, respectively, for  $\mu > 0$ . No attracting orbit exists in either side of  $\mu = 0$ .

**B. Border crossing bifurcation**

Region 8:  $-2\sqrt{\delta_L} > \tau_L > -(1 + \delta_L)$ ,  $0 < \tau_R < 1$

*(Flip repeller changes to regular attractor)*

For  $\mu < 0$ , there is a chaotic attractor for most part of the parameter space. The attractor is formed by the same mechanism as in Region 1, and has structure similar to that shown in Fig. 10 (the only difference is that  $\bar{R}^*$  is in the  $L$  side).

However, since any initial condition anywhere in the state space must ultimately move to  $R$  and converge onto the attractor, the basin of attraction spans the whole state space.

For some parts of the parameter space within this region, high periodic attractors can exist. To investigate how one type of attractor changes to another, the bifurcation diagram for  $\mu < 0$  with  $\tau_R$  as parameter is shown in Fig. 14.

From the period-3 orbit a period-6 orbit is created due to a period doubling bifurcation and subsequently one of the period-6 fixed points hits the border which gives rise to a chaotic attractor. From the chaotic attractor a period-4 orbit is originated due to border collision pair bifurcation in the fourth iterate. From period-4 a transition to period-8 occurs due to period doubling bifurcation and subsequently one of the period-8 fixed points collides with the border to give rise to a chaotic attractor. The same kind of bifurcation phenomena is observed if we vary  $\tau_L$  within this parameter region.

For  $\mu > 0$ ,  $R^*$  is a regular attractor. All the initial conditions in  $R$  side converge on to  $R^*$  and all the initial conditions in  $L$  are repelled to the  $R$  side and gradually converge on to  $R^*$ . So we get a period-1 attractor for  $\mu > 0$ , and its basin also spans the whole space.

Region 9:  $-2\sqrt{\delta_L} > \tau_L > -(1 + \delta_L)$ ,  $-1 < \tau_R < 0$

*(Flip repeller changes to flip attractor)*

In this region for  $\mu < 0$ ,  $L^*$  is a flip repeller. High periodic orbits (e.g., period-3, period-5 or higher periods) or chaotic attractor may exist. The bifurcation diagram for  $\mu < 0$  with  $\tau_L$  as the parameter is shown in Fig. 15. It is found that the high-periodic orbits are all born with one point on the border—therefore these are border collision pair bifurcations of higher iterates. The changeover to chaos also occurs when one point of a high periodic orbit hits the border. Whenever attractors exist, their basin spans the whole space.

For  $\mu > 0$ ,  $R^*$  is a flip attractor and we get a stable period-1 orbit. Therefore in this region, as  $\mu$  is varied from a positive to a negative value, there is a bifurcation from a period-1 attractor to a high periodic attractor or chaos.

Region 10:  $\tau_L < -(1 + \delta_L)$ ,  $0 < \tau_R < 1$

*(Flip saddle changes to regular attractor)*

For  $\mu < 0$ ,  $L^*$  is a flip saddle. Initial conditions in  $R$  move towards the regular attractor  $\bar{R}^*$  which is in  $L$ , and initial conditions in  $L$  flip to  $R$  due to the action of  $L^*$ . This

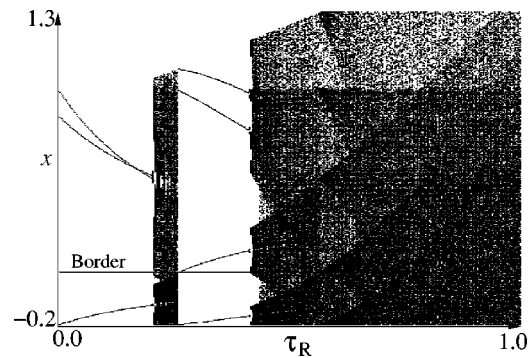


FIG. 14. The bifurcation diagram for Region 8 in positive determinant case with  $\tau_R$  as parameter (varied from 0.15 to 0.5), and  $\tau_L = -4.5$ ,  $\delta_L = 4$ ,  $\delta_R = 0$ , and  $\mu = -0.2$ .

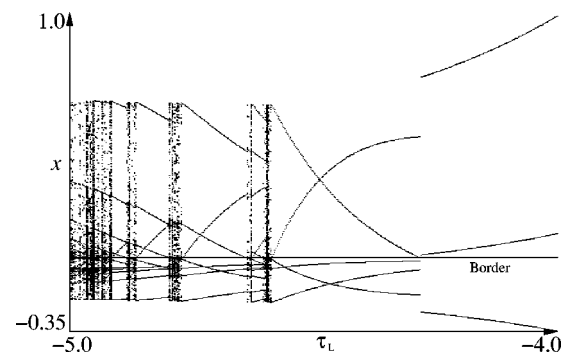


FIG. 15. The bifurcation diagram for Region 9 in positive determinant case with  $\tau_L$  as parameter (varied from  $-5.0$  to  $-4.0$ ). The other parameters are  $\tau_R = -0.9$ ,  $\delta_L = 4$ ,  $\delta_R = 0$ , and  $\mu = -0.2$ .

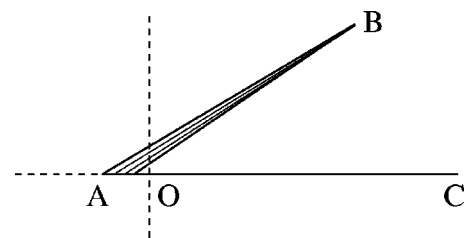


FIG. 16. The chaotic attractor for Region 10 in positive determinant case with  $\tau_L = -6$ ,  $\delta_L = 4$ ,  $\tau_R = 0.9$ , and  $\delta_R = 0$ .

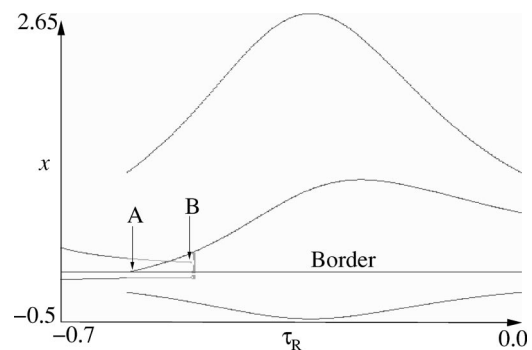


FIG. 17. The bifurcation diagram for Region 11 in positive determinant case with  $\tau_R$  as parameter (varied from  $-0.7$  to  $0.0$ ) and  $\tau_L = -6.0$ ,  $\delta_L = 4$ ,  $\delta_R = 0$ , and  $\mu = -0.2$ .

creates the possibility of high period orbits or chaos. The bifurcation diagram is similar to the one shown in Fig. 14, and exhibit the same phenomenology. The structure of the chaotic attractor is shown in Fig. 16. The extremities of the attractor are formed by  $O \mapsto A$ ,  $A \mapsto B$  and  $B \mapsto C$ . The forward iterates of  $OA$  forms the attractor as shown in this figure.

For  $\mu > 0$ ,  $R^*$  is a regular attractor. All the initial conditions in the  $R$  side converge on to  $R^*$ .  $\bar{L}^*$  is a flip saddle which is in the  $R$  side. All the initial conditions in the  $L$  side flip to the  $R$  side and finally converge onto  $R^*$ . So we get a unique period-1 attractor.

Region 11:  $\tau_L < -(1 + \delta_L)$ ,  $-1 < \tau_R < 0$   
 (Flip saddle changes to flip attractor)

For  $\mu < 0$ ,  $L^*$  is a flip-saddle and  $\bar{R}^*$  is a flip attractor—both located in the  $L$  side. For  $\mu < 0$  there may be period-2, period-3 or chaotic attractor. Coexisting attractors may also exist. The bifurcation diagram is shown in Fig. 17, which shows the evolution of the coexisting attractors. A period-3 orbit is created due to pair bifurcation at bifurcation point “A.” A period-2 orbit coexists so long as (9) and (10) are satisfied. If  $\tau_R$  is decreased, as (10) is violated, the period-2 orbit goes through period-doubling at “B.” Subsequently one of the bifurcated orbits hits the border and at the ensuing border crossing bifurcation, a chaotic orbit develops. As the parameter  $\tau_R$  is increased, the separation between the two period-2 fixed points gradually increases and finally becomes infinite (not shown in Fig. 17). So for some value of the parameter the attractor does not exist.

For  $\mu > 0$ ,  $R^*$  is a flip attractor and  $\bar{L}^*$  is a flip saddle. All the initial conditions in the  $R$  side converge onto  $R^*$  and all the initial conditions in the  $L$  side flip to the  $R$  side due to the action of the  $\bar{L}^*$  and finally converge onto  $R^*$ . So a period-1 attractor exists for  $\mu > 0$ .

Region 12:  $-2\sqrt{\delta_L} < \tau_L < 2\sqrt{\delta_L}$ ,  $0 < \tau_R < 1$   
 (Repelling spiral changes to regular attractor)

In this region of the parameter space  $L^*$  is a repelling spiral. For  $-2\sqrt{\delta_L} < \tau_L < 0$ , it has counter-clockwise sense of rotation while for  $0 < \tau_L < 2\sqrt{\delta_L}$  it has clockwise sense of rotation.  $\bar{R}^*$  is a regular attractor and is in the  $L$  side for  $\mu < 0$ , which makes all initial conditions in  $R$  move towards  $L$  along the  $x$ -axis. The effect of the spiral fixed point makes them to go back to  $R$  in some iterate and this causes high periodic orbits or a chaotic attractor to exist for  $\mu < 0$ .

A few different types of chaotic attractors observed in this region are shown in Fig. 18 which are formed in the following manner. In Fig. 18(a)  $O \mapsto B \mapsto A \mapsto D$  and  $E \mapsto C$ . This forms the extremities of the attractor. The segments  $OB \mapsto BA$ ,  $BE \mapsto AC$ ,  $EA \mapsto CD$ . Keeping other parameters fixed as  $\tau_L$  is increased we find a 4-piece chaotic attractor as shown in Fig. 18(b) where  $O \mapsto B \mapsto A \mapsto D \mapsto C \mapsto E \mapsto I \mapsto H \mapsto F \mapsto G \mapsto J$  and  $J$  maps to a point on  $HD$ . As  $\tau_L$  is further increased we get an attractor as shown in Fig. 18(c) where the extremities are formed in this manner:  $O \mapsto B \mapsto A \mapsto C$ . For different set of  $\tau_L$ ,  $\tau_R$  and  $\delta_L$  values we get attractors of different shape. One example is shown in Fig. 18(d) where origin  $O \mapsto B \mapsto A \mapsto D \mapsto F$  and  $E \mapsto C$ .

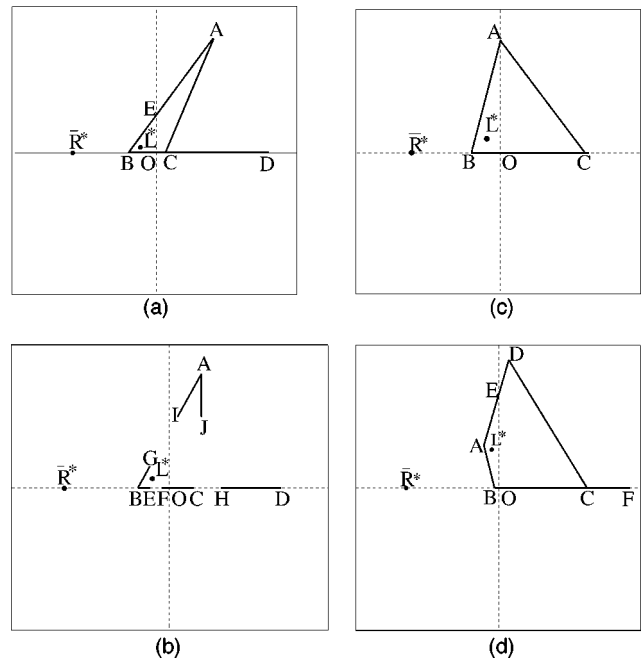


FIG. 18. Chaotic attractors of different shapes for different combinations of the parameters for Region 12 in positive determinant case. (a)  $\tau_L = -3$ ,  $\tau_R = 0.5$ ,  $\delta_L = 4$ ,  $\delta_R = 0$ , and  $\mu = -0.2$ . (b)  $\tau_L = -2$ ,  $\tau_R = 0.5$ ,  $\delta_L = 4$ ,  $\delta_R = 0$ , and  $\mu = -0.2$ . (c)  $\tau_L = -1$ ,  $\tau_R = 0.5$ ,  $\delta_L = 4$ ,  $\delta_R = 0$ , and  $\mu = -0.2$ . (d)  $\tau_L = 2$ ,  $\delta_L = 9$ ,  $\tau_R = 0.8$ ,  $\delta_R = 0$ , and  $\mu = -0.05$ .

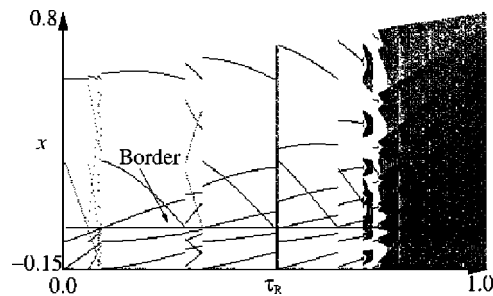


FIG. 19. The bifurcation diagram for Region 12 in positive determinant case with  $\tau_R$  as the parameter (varied from 0 to 1) and  $\tau_L = 2$ ,  $\delta_L = 9$ ,  $\delta_R = 0$ , and  $\mu = -0.05$ .

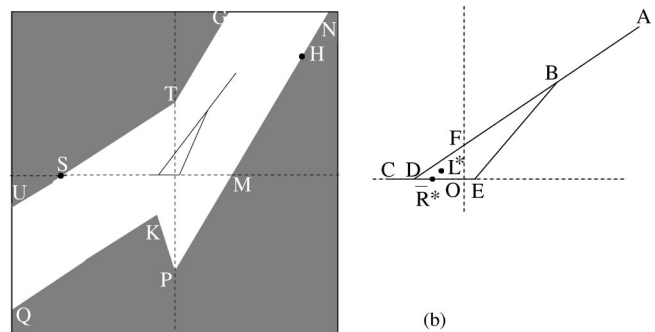


FIG. 20. Chaotic attractor for Region 13 in positive determinant case with  $\tau_L = -3.0$ ,  $\tau_R = -1.7$ ,  $\delta_L = 4$ ,  $\delta_R = 0$ , and  $\mu = -0.1$ .

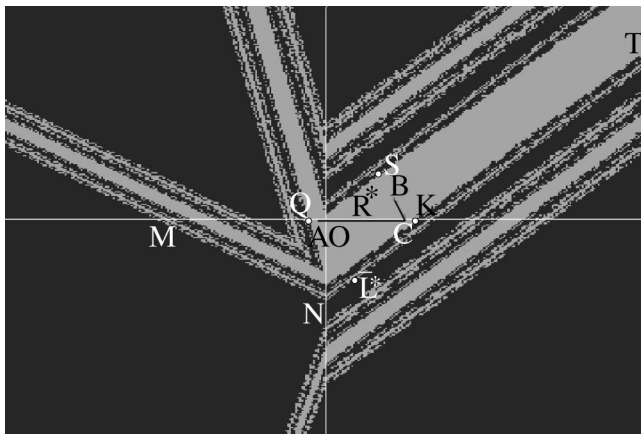


FIG. 21. The basin boundary and the chaotic attractor for Region 13 in positive determinant case with  $\tau_L=1.5$ ,  $\tau_R=-1.2$ ,  $\delta_L=4$ ,  $\delta_R=0$ , and  $\mu=0.1$ .

The basin of attraction spans the whole state space. In all the cases  $L^*$  lies within the attractor. One important feature of these chaotic attractors is that they are organized by a spiral repeller and a virtual attracting fixed point, and hence do not occur on the unstable manifold of a saddle. The sensitive dependence on initial condition is caused by the repeller.

To investigate the transitions between high periodic orbits and chaotic orbits, the bifurcation diagram is shown in Fig. 19. It is seen that repeated border collisions cause the transitions between various periodic orbits and chaos. At some bifurcation points the periodic orbit goes through period doubling and subsequently one of the points hits the border to give rise to chaotic attractor. Subsequently, high periodic orbits are created due to border collision pair bifurcation.

For  $\mu > 0$ ,  $R^*$  is a regular attractor and a stable period-1 orbit exists.

Region 13:  $-2\sqrt{\delta_L} < \tau_L < 2\sqrt{\delta_L}$ ,  $\tau_R < -1$   
 (Repelling spiral changes to flip saddle)

It can be seen from (8) that for  $\tau_L \tau_R < (1 + \delta_L)$  the period-2 orbit exists for  $\mu > 0$ , while for  $\tau_L \tau_R > (1 + \delta_L)$  it

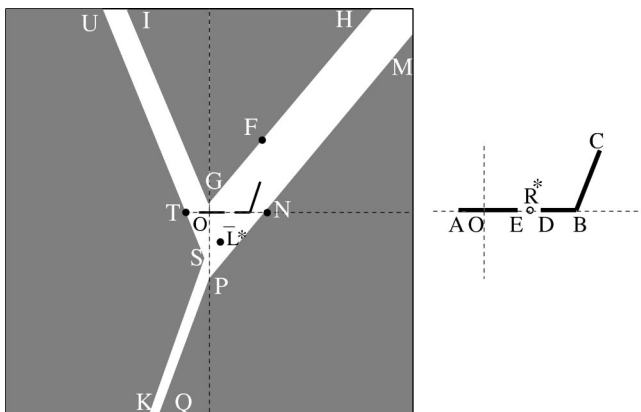


FIG. 22. The basin boundary and the chaotic attractor for Region 13 in positive determinant case for  $\tau_L=-1.0$ ,  $\tau_R=-1.2$ ,  $\delta_L=4$ ,  $\delta_R=0$ , and  $\mu=0.1$ .

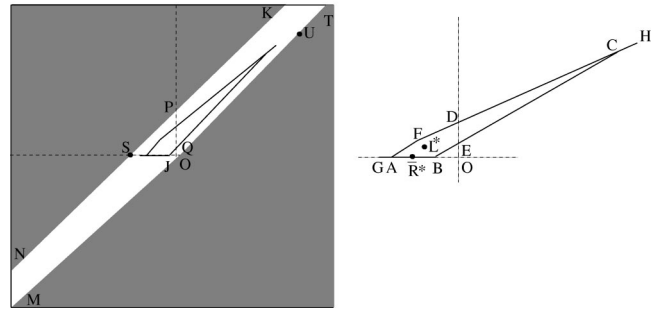


FIG. 23. Chaotic attractors for Region 14 in positive determinant case with  $\tau_L=-4.62$ ,  $\tau_R=-1.1$ ,  $\delta_L=4$ ,  $\delta_R=0$ , and  $\mu=-0.1$ .

exists for  $\mu < 0$ . Condition (9) implies that in a part of Region 13 there is a subcritical period doubling caused by border collision.

For  $\mu < 0$ ,  $L^*$  is a repelling spiral. A high periodic orbit or a chaotic attractor may exist, which may be annihilated in some parts of the parameter space due to boundary crisis. Chaotic attractors of different shapes exist for different values of the parameter.

One such attractor and its basin of attraction are shown in Fig. 20.  $H$  and  $S$  are the locations of the fixed points of the second iterate, which is a saddle. The basin boundary is formed by the stable manifold of this second iterate fixed point. The stable eigenvector at  $S$  is along  $UT$ , and the stable eigenvector at  $H$  is  $NHP$ —which fold at the intersections with the  $y$ -axis, forming the stable manifold:  $ST \rightarrow NM$ ,  $PN \rightarrow S$ , and  $M \rightarrow S$ . The stable manifold bends at  $T$  and the preiterate of  $T$  is  $K$  which is also a fold point. The extremities of the chaotic attractor are formed in the following manner. Origin  $O \rightarrow D$ ,  $D \rightarrow B$ ,  $F \rightarrow E$ ,  $E \rightarrow C$ ,  $C \rightarrow A$  and  $A$  maps to a point on  $DC$ . For some parameter ranges within this region, the separation between the period-2 saddle that forms the basin boundary increases to large dimension, and hence the basin becomes very large.

As  $\tau_R$  is decreased or  $\tau_L$  is increased within this region, high periodic orbits and chaotic attractors exist, each with a different condition of occurrence of boundary crisis. This gives the fine structure of the parameters space as shown in Fig. 9(a).

For  $\mu > 0$ , there can be period-2 [when (9) and (10) are satisfied], high periodic orbit, chaotic attractor or no attrac-

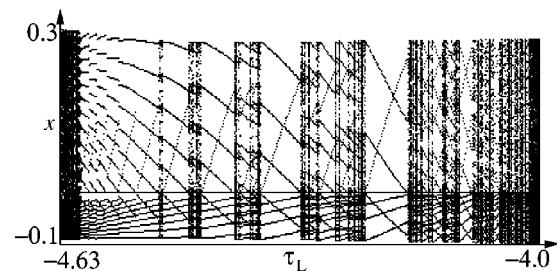


FIG. 24. The bifurcation diagram for Region 14 in positive determinant case with  $\tau_L$  as parameter (varied from  $-4.63$  to  $-4.0$ ) and  $\tau_R=-1.1$ ,  $\delta_L=4$ ,  $\delta_R=0$ , and  $\mu=-0.1$ .

TABLE III. The nature of the fixed points and the type of bifurcations for  $\delta_L > 1$  and  $\delta_R = 0$ .

Region	$\mu < 0$	$\mu > 0$	Type of bifurcation
Border collision pair bifurcations			
Region 1: $\tau_R > 1$ , $-2\sqrt{\delta_L} > \tau_L > -(1 + \delta_L)$	$L^*$ -flip repeller $R^*$ -regular saddle	No fixed point	Birth of a stable chaotic attractor, or no attractor for $\mu < 0$
Region 2: $\tau_R > 1$ , $\tau_L < -(1 + \delta_L)$	$L^*$ -flip saddle $R^*$ -regular saddle	No fixed point	Birth of a chaotic attractor, or no attractor for $\mu < 0$
Region 3: $\tau_R < -1$ , $\tau_L > (1 + \delta_L)$	No fixed point	$L^*$ -regular saddle $R^*$ -flip saddle	Birth of a chaotic attractor, or no attractor for $\mu > 0$
Region 4: $0 < \tau_R < 1$ , $\tau_L > (1 + \delta_L)$	No fixed point	$L^*$ -regular saddle $R^*$ -regular attractor	Birth of a period-1 attractor for $\mu > 0$
Region 5: $-1 < \tau_R < 0$ , $\tau_L > (1 + \delta_L)$	No fixed point	$L^*$ -regular saddle $R^*$ -flip attractor	Birth of a period-1 attractor for $\mu > 0$
Region 6: $\tau_R > 1$ , $-2\sqrt{\delta_L} < \tau_L < 2\sqrt{\delta_L}$	$L^*$ -repelling spiral $R^*$ -regular saddle	No fixed point	Birth of a chaotic attractor, or high periodic orbit, or no attractor for $\mu < 0$
Region 7: $\tau_R > 1$ , $2\sqrt{\delta_L} < \tau_L < (1 + \delta_L)$	$L^*$ -regular repeller $R^*$ -regular saddle	No fixed point	No attractor for any value of $\mu$
Border crossing bifurcations			
Region 8: $0 < \tau_R < 1$ , $-(1 + \delta_L) < \tau_L < -2\sqrt{\delta_L}$	$L^*$ -flip repeller	$R^*$ -regular attractor	High periodic orbit or chaos for $\mu < 0$ and period-1 for $\mu > 0$
Region 9: $-1 < \tau_R < 0$ , $-(1 + \delta_L) < \tau_L < -2\sqrt{\delta_L}$	$L^*$ -flip repeller	$R^*$ -flip attractor	High periodic orbit or chaos for $\mu < 0$ and period-1 for $\mu > 0$
Region 10: $0 < \tau_R < 1$ , $\tau_L < -(1 + \delta_L)$	$L^*$ -flip saddle	$R^*$ -regular attractor	High periodic orbit or chaos for $\mu < 0$ and period-1 for $\mu > 0$
Region 11: $-1 < \tau_R < 0$ , $\tau_L < -(1 + \delta_L)$	$L^*$ -flip saddle	$R^*$ -flip attractor	Period-2, high-period orbit or chaos plus coexisting attractor for $\mu < 0$ and period-1 for $\mu > 0$
Region 12: $0 < \tau_R < 1$ , $-2\sqrt{\delta_L} < \tau_L < 2\sqrt{\delta_L}$	$L^*$ -repelling spiral	$R^*$ -regular attractor	High periodic orbit or chaos for $\mu < 0$ and period-1 for $\mu > 0$
Region 13: $\tau_R < -1$ , $-2\sqrt{\delta_L} < \tau_L < 2\sqrt{\delta_L}$	$L^*$ -repelling spiral	$R^*$ -flip saddle	High periodic orbit or chaotic attractor or no attractor for $\mu < 0$ and period-2, high periodic orbit or chaotic attractor for $\mu > 0$
Region 14: $\tau_R < -1$ , $-(1 + \delta_L) < \tau_L < -2\sqrt{\delta_L}$	$L^*$ -flip repeller	$R^*$ -flip saddle	High periodic orbit or chaotic attractor or no attractor for $\mu < 0$ and period-2 or no attractor for $\mu > 0$
Region 15: $\tau_R < -1$ , $2\sqrt{\delta_L} < \tau_L < (1 + \delta_L)$	$L^*$ -regular repeller	$R^*$ -flip saddle	No attractor for $\mu < 0$ and chaotic attractor or no attractor for $\mu > 0$
Region 16: $-1 < \tau_R < 0$ , $-2\sqrt{\delta_L} < \tau_L < 2\sqrt{\delta_L}$	$L^*$ -repelling spiral	$R^*$ -flip attractor	High periodic orbit plus coexisting attractor or no attractor for $\mu < 0$ and period-1 for $\mu > 0$
Region 17: $0 < \tau_R < 1$ , $2\sqrt{\delta_L} < \tau_L < (1 + \delta_L)$	$L^*$ -regular repeller	$R^*$ -regular attractor	No attractor for $\mu < 0$ and period-1 for $\mu > 0$
Region 18: $-1 < \tau_R < 0$ , $2\sqrt{\delta_L} < \tau_L < (1 + \delta_L)$	$L^*$ -regular repeller	$R^*$ -flip attractor	No attractor for $\mu < 0$ and period-1 for $\mu > 0$
Region 19: $\tau_R > 1$ , $\tau_L > (1 + \delta_L)$	$L^*$ -regular saddle	$R^*$ -regular saddle	No attractor for any value of $\mu$
Region 20: $\tau_R < -1$ , $\tau_L < -(1 + \delta_L)$	$L^*$ -flip saddle	$R^*$ -flip saddle	No attractor for any value of $\mu$

tor.  $R^*$  is a flip saddle situated in  $R$  side, and  $\bar{L}^*$  is a repelling spiral also in the  $R$  side.

If  $\bar{L}^*$  is a clockwise rotating spiral repeller (which happens for  $0 < \tau_L < 2\sqrt{\delta_L}$ ) then the basin boundary, formed by the stable manifold of the third iterate fixed point, assumes a fractal structure as shown in Fig. 21.  $Q$ ,  $K$  and  $S$  are the locations of the fixed point of the third iterate. The unstable manifold is along the  $x$ -axis. The stable manifold at  $K$  is along  $TK$  which folds at  $N$  and intersects the unstable manifold (i.e.,  $x$ -axis) at  $M$ . One intersection between stable and unstable manifold signifies an infinite number of intersections. So the basin boundary takes fractal structure. Boundary crisis may lead to the annihilation of the chaotic attractor when point  $C$  touches the basin boundary.

However, the character of the attractor and that of the basin boundary are not always the same as shown in Figs. 22 and 23. The chaotic attractor has two disjoint pieces for this setting of the parameters. The extremities of the attractor are formed in this manner:  $O \mapsto B$ ,  $B \mapsto A$ ,  $A \mapsto C$ ,  $C \mapsto E$ ,  $E \mapsto D$ , and  $D$  maps to a point on  $AE$ . The chaotic attractor is annihilated due to boundary crisis at a certain parameter value.

The basin boundary is formed by the stable manifold of the third iterate fixed point which is a saddle.  $F$ ,  $N$ ,  $T$  are the locations of the third iterate fixed points and the stable eigenvector at  $T$  is along  $SU$ , which folds at every intersection with the  $y$ -axis and their preiterates, thus forming the stable manifold. In this case there is no homoclinic intersection and

TABLE IV. The nature of the fixed points and the type of bifurcations for  $-1 < \delta_L < 0$  and  $\delta_R = 0$ .

Region	$\mu < 0$	$\mu > 0$	Type of bifurcation
Border collision pair bifurcations			
Region 1: $\tau_R > 1$ , $\tau_L < -(1 + \delta_L)$	$L^*$ -flip saddle $R^*$ -regular saddle	No fixed point	Birth of period-2 attractor, or chaotic attractor, or unstable chaotic orbit for $\mu < 0$
Region 2: $\tau_R > 1$ , $-(1 + \delta_L) < \tau_L < (1 + \delta_L)$	$L^*$ -flip attractor $R^*$ -regular saddle	No fixed point	Birth of a period-1 attractor for $\mu < 0$
Region 3: $0 < \tau_R < 1$ , $\tau_L > (1 + \delta_L)$	No fixed point	$L^*$ -flip saddle $R^*$ -regular attractor	Birth of a period-1 attractor for $\mu > 0$
Region 4: $-1 < \tau_R < 0$ , $\tau_L > (1 + \delta_L)$	No fixed point	$L^*$ -flip saddle $R^*$ -flip attractor	Birth of a period-1 attractor for $\mu > 0$
Region 5: $\tau_R < -1$ , $\tau_L > (1 + \delta_L)$	No fixed point	$L^*$ -flip saddle $R^*$ -flip saddle	Birth of a period-2 or chaotic attractor or no attractor for $\mu > 0$
Border crossing bifurcations			
Region 6: $\tau_R > 1$ , $\tau_L > (1 + \delta_L)$	$R^*$ -regular saddle	$L^*$ -flip saddle	No attractor for any value of $\mu$
Region 7: $0 < \tau_R < 1$ , $\tau_L < -(1 + \delta_L)$	$L^*$ -flip saddle	$R^*$ -regular attractor	Period-2, or chaotic attractor for $\mu < 0$ and period-1 attractor for $\mu > 0$
Region 8: $0 < \tau_R < 1$ , $-(1 + \delta_L) < \tau_L < (1 + \delta_L)$	$L^*$ -flip attractor	$R^*$ -regular attractor	period-1 for any value of $\mu$
Region 9: $-1 < \tau_R < 0$ , $\tau_L < -(1 + \delta_L)$	$L^*$ -flip saddle	$R^*$ -flip attractor	Period-2 or no attractor for $\mu < 0$ , period-1 for $\mu > 0$
Region 10: $-1 < \tau_R < 0$ , $-(1 + \delta_L) < \tau_L < (1 + \delta_L)$	$L^*$ -flip attractor	$R^*$ -flip attractor	period-1 for any value of $\mu$
Region 11: $\tau_R < -1$ , $\tau_L < -(1 + \delta_L)$	$L^*$ -flip saddle	$R^*$ -flip saddle	No attractor for any value of $\mu$
Region 12: $\tau_R < -1$ , $-(1 + \delta_L) < \tau_L < (1 + \delta_L)$	$L^*$ -flip attractor	$R^*$ -flip saddle	Period-1 for $\mu < 0$ and period-2, or chaotic attractor or no attractor for $\mu > 0$

the basin boundary is composed of line segments.

Region 14:  $-(1 + \delta_L) < \tau_L < -2\sqrt{\delta_L}$ ,  $\tau_R < -1$   
(*Flip repeller changes to flip saddle*)

Due to condition (8), there is a supercritical period doubling if (9) is satisfied, and a subcritical period doubling if (9) is violated. For  $\mu < 0$ ,  $L^*$  is a flip repeller.  $\bar{R}^*$  is a flip saddle, and if (9) is violated the period-2 orbit exists but is unstable. Under such condition high periodic orbit or chaotic attractor may exist due to the same mechanism as discussed in Region 13 (Fig. 20).

The bifurcation diagram with  $\tau_L$  as the bifurcation parameter is shown in Fig. 24. We find that due to repeated border collision bifurcations the high periodic orbits or chaotic attractors are alternatively created—a phenomenon observed in many of the parameter space regions.

For  $\mu > 0$  we get period-2 orbit or no attractor in this parameter range. So long as (9) and (10) are satisfied period-2 orbit exists. But as the parameters are varied, a point is reached when (9) is violated and the separation between the period-2 fixed points becomes infinite and no period-2 orbit exists after that.

Region 15:  $2\sqrt{\delta_L} < \tau_L < (1 + \delta_L)$ ,  $\tau_R < -1$   
(*Regular repeller changes to flip saddle*)

For  $\mu < 0$   $L^*$  is a regular repeller and  $\bar{R}^*$  is a flip saddle. So all initial conditions in  $L$  are repelled away and initial conditions in  $R$  flip to  $L$  and then are repelled to infinity. Therefore no attractor exists in this region of the parameter space for  $\mu < 0$ .

For  $\mu > 0$   $R^*$  is a flip saddle and is in the  $R$  side. We get chaotic attractor which may become unstable at some parameter value. The structure of the chaotic attractor and the basin

boundary (formed by the stable manifold of the third iterate saddle) are similar to Fig. 21.

Region 16:  $-2\sqrt{\delta_L} < \tau_L < 2\sqrt{\delta_L}$ ,  $-1 < \tau_R < 0$   
(*Repelling spiral changes to flip attractor*)

For  $\mu < 0$ , there is a repelling spiral in  $L$  side. We get high periodic orbit or no attractor. Coexisting attractors may also exist. The initial conditions in the  $L$  side move to the  $R$  side after a finite number of iterations and as  $\bar{R}^*$  is a flip attractor the next iterate will be on the negative  $x$ -axis. Thus there exists a possibility of having stable high periodic orbits. It is possible to work out the conditions for existence of each high periodic orbit, but that results in cumbersome expressions which we omit here. It is however notable that the high periodic orbits are created due to pair bifurcation. Attractors exist in narrow strips [see Fig. 9(a)] in the parameters space due to the same phenomenology as discussed in Region 13.

For  $\mu > 0$   $R^*$  is a flip attractor, and we get a stable period-1 orbit.

Region 17:  $2\sqrt{\delta_L} < \tau_L < (1 + \delta_L)$ ,  $0 < \tau_R < 1$   
(*Regular repeller changes to regular attractor*)

Region 18:  $2\sqrt{\delta_L} < \tau_L < (1 + \delta_L)$ ,  $-1 < \tau_R < 0$   
(*Regular repeller changes to flip attractor*)

For  $\mu < 0$ ,  $L^*$  is regular repeller. All the initial conditions in  $L$  side either go to infinity due to the repelling action of  $L^*$  or moves to the  $R$  side. In the latter case it will fall on the  $x$ -axis in the next iterate and gradually move to the  $L$  side due to the action of  $\bar{R}^*$  and subsequently go to infinity due to the repelling action of  $L^*$ . So there will be no attractor for  $\mu < 0$ .

TABLE V. The nature of the fixed points and the type of bifurcations for  $0 < \delta_L < 1$  and  $\delta_R = 0$ .

Region	$\mu < 0$	$\mu > 0$	Type of bifurcation
Border collision pair bifurcations			
Region 1: $\tau_R > 1$ , $\tau_L < -(1 + \delta_L)$	$L^*$ -flip saddle $R^*$ -regular saddle	No fixed point	Birth of a stable chaotic attractor, or unstable chaotic orbit or no attractor for $\mu < 0$
Region 2: $\tau_R > 1$ , $-(1 + \delta_L) < \tau_L < -2\sqrt{\delta_L}$	$L^*$ -flip attractor $R^*$ -regular saddle	No fixed point	Birth of a period-1 attractor for $\mu < 0$
Region 3: $\tau_R > 1$ , $-2\sqrt{\delta_L} < \tau_L < 2\sqrt{\delta_L}$	$L^*$ -attracting spiral $R^*$ -regular saddle	No fixed point	Birth of a period-1 attractor for $\mu < 0$
Region 4: $\tau_R > 1$ , $2\sqrt{\delta_L} < \tau_L < (1 + \delta_L)$	$L^*$ -regular attractor $R^*$ -regular saddle	No fixed point	Birth of a period-1 attractor for $\mu < 0$
Region 5: $0 < \tau_R < 1$ , $\tau_L > (1 + \delta_L)$	No fixed point	$L^*$ -regular saddle $R^*$ -regular attractor	Birth of a period-1 attractor for $\mu > 0$
Region 6: $-1 < \tau_R < 0$ , $\tau_L > (1 + \delta_L)$	No fixed point	$L^*$ -regular saddle $R^*$ -flip attractor	Birth of a period-1 attractor for $\mu > 0$
Region 7: $\tau_R < -1$ , $\tau_L > (1 + \delta_L)$	No fixed point	$L^*$ -regular saddle $R^*$ -flip saddle	Birth of a stable chaotic attractor, or unstable chaotic attractor or no attractor for $\mu > 0$
Border crossing bifurcations			
Region 8: $\tau_R > 1$ , $\tau_L > (1 + \delta_L)$	$R^*$ -regular saddle	$L^*$ -regular saddle	No attractor for any value of $\mu$
Region 9: $0 < \tau_R < 1$ , $\tau_L < -(1 + \delta_L)$	$L^*$ -flip saddle	$R^*$ -regular attractor	Period-2 or chaos for $\mu < 0$ and period-1 for $\mu > 0$
Region 10: $0 < \tau_R < 1$ , $-(1 + \delta_L) < \tau_L < -2\sqrt{\delta_L}$	$L^*$ -flip attractor	$R^*$ -regular attractor	Period-1 plus coexisting attractors for $\mu < 0$ and period-1 for $\mu > 0$
Region 11: $0 < \tau_R < 1$ , $-2\sqrt{\delta_L} < \tau_L < 2\sqrt{\delta_L}$	$L^*$ -attracting spiral	$R^*$ -regular attractor	Period-1 plus coexisting attractor (if $-2\sqrt{\delta_L} < \tau_L < 0$ ) and period-1 (if $0 < \tau_L < 2\sqrt{\delta_L}$ ) for any value of $\mu$
Region 12: $0 < \tau_R < 1$ , $2\sqrt{\delta_L} < \tau_L < (1 + \delta_L)$	$L^*$ -regular attractor	$R^*$ -regular attractor	Period-1 for any value of $\mu$
Region 13: $-1 < \tau_R < 0$ , $\tau_L < -(1 + \delta_L)$	$L^*$ -flip saddle	$R^*$ -flip attractor	Period-2 plus coexisting attractor or no attractor for $\mu < 0$ and period-1 plus coexisting attractor for $\mu > 0$
Region 14: $-1 < \tau_R < 0$ , $-(1 + \delta_L) < \tau_L < -2\sqrt{\delta_L}$	$L^*$ -flip attractor	$R^*$ -flip attractor	Period-1 plus coexisting attractor for $\mu < 0$ and period-1 plus different coexisting attractor for $\mu > 0$
Region 15: $-1 < \tau_R < 0$ , $-2\sqrt{\delta_L} < \tau_L < 2\sqrt{\delta_L}$	$L^*$ -attracting spiral	$R^*$ -flip attractor	Period-1 (if $-2\sqrt{\delta_L} < \tau_L < 0$ ) and period-1 plus coexisting attractors (if $0 < \tau_L < 2\sqrt{\delta_L}$ ) for any value of $\mu$
Region 16: $-1 < \tau_R < 0$ , $2\sqrt{\delta_L} < \tau_L < (1 + \delta_L)$	$L^*$ -regular attractor	$R^*$ -flip attractor	Period-1 attractor for any value of $\mu$
Region 17: $\tau_R < -1$ , $\tau_L < -(1 + \delta_L)$	$L^*$ -flip saddle	$R^*$ -flip saddle	No attractor for any value of $\mu$
Region 18: $\tau_R < -1$ , $-(1 + \delta_L) < \tau_L < -2\sqrt{\delta_L}$	$L^*$ -flip attractor	$R^*$ -flip saddle	Period-1 for $\mu < 0$ and period-2 or no attractor for $\mu > 0$
Region 19: $\tau_R < -1$ , $-2\sqrt{\delta_L} < \tau_L < 2\sqrt{\delta_L}$	$L^*$ -attracting spiral	$R^*$ -flip saddle	Period-1 plus coexisting attractor for $\mu < 0$ and chaos or high periodic orbit plus coexisting attractor or period-2 plus coexisting attractor or no attractor for $\mu > 0$
Region 20: $\tau_R < -1$ , $2\sqrt{\delta_L} < \tau_L < (1 + \delta_L)$	$L^*$ -regular attractor	$R^*$ -flip saddle	Period-1 for $\mu < 0$ , period-2 or chaos for $\mu > 0$

For  $\mu > 0$  and  $\bar{L}^*$  is a regular repeller and  $R^*$  is a regular attractor (if  $0 < \tau_R < 1$ ) or flip attractor (if  $-1 < \tau_R < 0$ ). All the initial conditions in the  $R$  side will converge on to  $R^*$ . All the initial conditions in the  $L$  side will come to the  $R$  side due to the repelling action of  $\bar{L}^*$  and finally converge on to  $R^*$ . So there will be a stable period-1 attractor for  $\mu > 0$ .

Region 19:  $\tau_L > (1 + \delta_L)$ ,  $\tau_R > 1$   
(Regular saddle changes to regular saddle)

Region 20:  $\tau_L < -(1 + \delta_L)$ ,  $\tau_R < -1$   
(Flip saddle changes to flip saddle)

For  $\mu < 0$ , all initial conditions go to infinity along the

unstable eigenvector of  $L^*$  and for  $\mu > 0$ , all initial conditions go to infinity along the unstable eigen vector of  $R^*$ . Therefore there will be no attractor for both sides of  $\mu = 0$ .

Table III summarizes the various bifurcations occurring when  $\delta_L > 1$  and  $\delta_R = 0$ .

### VI. WHEN THE DETERMINANT LIES BETWEEN $-1$ AND $+1$

In Ref. 5 the border collision bifurcations were investigated under the condition that the determinants of the Jacobian matrices at the two sides of a border collision event lie

between  $-1$  and  $+1$ . Since a two-dimensional map with determinant zero is a one-dimensional map, the above work gives proper prediction of the border collision events under the special case where the determinant in one side is zero. Therefore, without describing each individual case, we summarize in Tables IV and V, and the results obtained from Ref. 5 regarding the  $\delta_R=0$  situation.

## VII. CONCLUSIONS

In this paper we have presented the border collision bifurcation phenomena that occur in piecewise smooth maps which are two dimensional in one side of the borderline and one dimensional in the other side. It has recently been found that such a situation occurs in systems of practical interest, most important examples coming from switching circuits. The theory developed in this paper will help in understanding the dynamics and bifurcation phenomena in such systems.

The study has indicated that very complicated bifurcation structures may exist under this condition, caused by repeated border collisions and changing conditions of occurrence of boundary crisis. Generally in two-dimensional

maps, chaotic attractors are known to occur only on the unstable manifold of saddles. The present study has shown that chaotic attractors can also be organized around repellers, and need not be associated with saddle fixed points.

<sup>1</sup>H. E. Nusse and J. A. Yorke, *Physica D* **57**, 39–57 (1992).

<sup>2</sup>G. Yuan, S. Banerjee, E. Ott, and J. A. Yorke, *IEEE Trans. Circuits Syst., I: Fundam. Theory Appl.* **45**, 707–715 (1998).

<sup>3</sup>S. Banerjee, E. Ott, J. A. Yorke, and G. H. Yuan, *IEEE Power Electronics Specialists's Conference*, 1997.

<sup>4</sup>S. Banerjee, M. S. Karthik, G. Yuan, and J. A. Yorke, *IEEE Trans. Circuits Syst., I: Fundam. Theory Appl.* **47**, 389–394 (2000).

<sup>5</sup>S. Banerjee, P. Ranjan, and C. Grebogi, *IEEE Trans. Circuits Syst., I: Fundam. Theory Appl.* **47**, 633–643 (2000).

<sup>6</sup>M. di Bernardo, M. I. Feigin, S. J. Hogan, and M. E. Homer, *Chaos, Solitons Fractals* **10**, 1881–1908 (1999).

<sup>7</sup>S. Banerjee and K. Chakrabarty, *IEEE Trans. Power Electron.* **13**, 252–260 (1998).

<sup>8</sup>C. K. Tse, *IEEE Trans. Circuits Syst., I: Fundam. Theory Appl.* **41**, 16–23 (1994).

<sup>9</sup>*Nonlinear Phenomena in Power Electronics*, edited by S. Banerjee and G. C. Verghese (IEEE, New York, 2001).

<sup>10</sup>S. Parui and S. Banerjee, Bifurcations due to transition from continuous conduction mode to discontinuous conduction mode in the boost converter (communicated).